University of Stavanger

Faculty of Science and Technology

MASTER'S THESIS

Study program/ Specialization: MSc Petroleum Engineering/ Reservoir Engineering	Spring semester, 2014 Open access
Writer: Gebremedhin Okbit Berhe	…… (Writer's signature)
Faculty supervisor: Professor Svein M Skjæveland External supervisor(s):	
Thesis title: Correct sampling of gas condensate reservoir with liquid drop around the well.	
Credits (ECTS): 30	
Key words: Infinite-acting period Gas condensate reservoir Black oil model Producing oil-gas ratio Eclipse 300 Eclipse 100	Pages: ……79…… + enclosure: 0 Stavanger, …….. Date/year

Universitetet
i Stavanger

Master Thesis

Correct Sampling Of Gas-Condensate Reservoir With Liquid Drop Around The well

By

Gebremedhin Okbit Berhe

Supervisor: Professor Svein M Skjæveland

Faculty of Engineering and Science
University of Stavanger

Abstract:

In gas-condensate system for an accurate engineering and science computations such as reserves estimation and well testing and analysing a concrete knowledge of phase and fluid phase behaviour is very significant.

In typical gas-condensate reservoirs with the decrease of the flowing bottom-hole pressure below the dew point dramatic decrease in gas production occurs. In presence of high pressure and temperature, there is a much higher tendency of complex organic molecules degradation. The conversion of these complex organic molecules into gas-condensate is highly dependent on their burial depth i.e the higher burial depth the higher probability of conversion. The gas-condensate reservoir contains only small part of heavier components but consists mainly of lighter components and methane. But looking in a general way, during degradation of organic complex molecules higher proportions of light HC components occur in deeper reservoirs. In most gas-condensate reservoir cases variation in the composition with time may tend to make some confusion in understanding phase and flow behaviors.

In this study, we have used a single-layered, radial and two-dimensional gas condensate and black-oil reservoir models and we have performed both compositional and black-oil isothermal flow simulations. As most studies inform in low permeable gas condensate reservoirs once the pressure drops below the dew-point pressure, then getting accurate fluid sampling is highly challenging. One of the minor observations in this study was that the producing OGR stabilizes quickly below the initial OGR throughout the entire infinite-acting period as long as we kept avoiding BHP from going below the targeting minimum BHP in order to prevent the sharp rate depletion.

The major aims of this thesis were make some investigations on how to test a gas-condensate and oil reservoirs in such a way that could give us a correct rate and to observe at which rate we should take our sample. We have concluded that when a liquid dropout from a gas the LGR will always decrease in dependent of the rate. Therefore, the safe way to precise sampling is at a lower rate.

Acknowledgements

Firstly, I would like to give my deepest appreciation and gratitude to *Professor Svein M Skjæveland (University of Stavanger)* for his tireless support and excellent guidance through out the entire thesis work.

Special thanks to my mother and father Lawyer Berhe Gebremedhin for being supportive and for their encouragement in my academic life ever since my childhood.

I would also like to thank my colleagues in Archer the well company AS and Logtek AS for their support and flexibility in my working hours and their endless encouragement.

Thanks to my big role models engineer Tesfalem Kesete Ghebreab (Senior advisor Skatteetatens IT og servicepartner), Million Berhe (Kitron AS, Arendal) and Feven Berhe for being supportive, good guidance and their help.

Finally, my most heartfelt gratitude goes to my loving family.

Content

Chapter 1.

1.1 Introduction

This paper explains some of the behaviours of gas condensate reservoirs and an oil reservoir. Gas-condensate fields are nowadays-quite commonplace on the Norwegian North Sea (Sleipner, Trym, Atl and so on). As most studies confirmed the gas-condensate economic importance and the frequency at which they are being detected have significantly increased in the petroleum industry. Most gas-condensate reservoirs show complex phase and flow behaviors due to the existence of condensate banking in the near well region and their behaviours are usually shown by the production of stock-tank oil and surface gas. The typical range of surface condensate is somewhere between 10 to 300 STB/MMscf . These reservoirs normally have a temperature between critical point and the cricondentherm on the reservoir fluid's PT diagram (figure 1.1) and it is the most accurate means of identifying them.

It is essential to have a wide understanding of the flow and phase behaviour in order to make correct computations and perform some simulations for gas-condensates. During the discovery, a typical gas-condensate field pressure is somewhere above or closer to the critical pressure. Initially when the gas-condensate reservoir is at reservoir conditions it only contains single-phase gas. Gas-condensate reservoirs mostly produce gases with some liquid dropout occurring in the separator. Then liquid condenses from the gas as the gas further flows through the reservoir and production tubing and finally through the surface separator. Condensate dropout occurs in the reservoir as the pressure in the reservoir falls below the dewpoint as a consequence the production decreases significantly and the liquids condensed in the reservoir are unrecoverable. In gas-condensate reservoirs condensate saturations and liquid dropout are significant parameters. The liquid dropout initially occurs near the wellbore and further propagates radially away from the well relative to the pressure drop. The figure

below (figure 1.1) shows the typical Pressure and Temperature (PT) fluid's phase diagram.

John Evans and Reggie (1998) have mentioned some of the reasons for the reduction of well productivity. That is, large reduction in well productivity can occur in gas-condensate reservoirs during pressure depletion due to the build-up of a condensate saturation ring near the wellbore. The relative permeability to gas decreases with an increase of gas-condensate saturation, which leads to the productivity loss. The productivity loss occurs when the reservoir pressure starts to fall below the dew point, however the productivity loss can occur very fast due to high-pressure drawdown in the near wellbore region.

If we compare the gas-condensate reservoir with dry-gas reservoir, there are several factors that affect the performance of gas-condensate fields at the time of exploration process. Øivind Fevang (1995) explained the main difference between "gas" and "gas-condensate" reservoirs with respect to the phase behaviours and well deliverability. There will not be any liquid condensation in the gas reservoir since the gas reservoir does not experience two-hydrocarbon phase at the reservoir condition. Unlike gas-condensate reservoir, a gas reservoir will not have significant condensable surface liquids to "loose" due to retrograde condensation. Another main difference is the loss in the well deliverability experienced by gas-condensate reservoirs, because of the build-up of liquid saturation near the wellbore (gas deliverability loss due to condensate blockage).

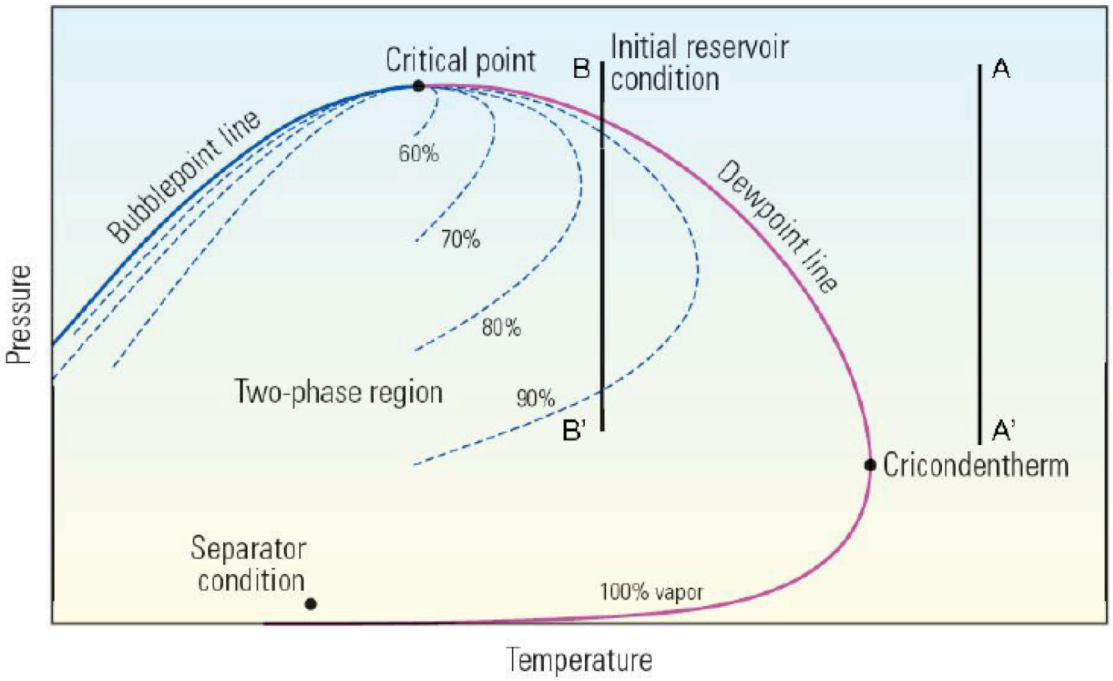

Figure 1.1: Typical gas-condensate fluid phase diagram (Fan et al., 2005).

The curve line indicates the changes as the fluid cools flowing up the wellbore and into the separator whereas; the vertical line indicates the phase changes in the reservoir. In both cases, liquid starts to drop out as the pressure falls below the dew point.

Afidick , D Kaczorowski and Bette (1994) indicated that the productivity loss caused by condensate build-up is striking and in some situations the decline can be as high as a factor of 2 to 4. In cases where very lean gas-condensates occur with a maximum liquid drop out of 1%, the productivity maybe decreased by a factor of two as the pressure drops below the dew point pressure.

Curtis Whitson (2012) made a statement that *what we produce at the surface is not what we have in the reservoir*. In his study, he has explained that a conventional reservoir produces much more oil than a liquid rich shale (LRS) oil reservoir that is initially saturated with oil ($S_{oi} = 1 - S_{wc}$) with equal amount of drawdown. He also discussed that the producing OGR (r_p) is more or less constant for a limited amount of period both for a gas well and LRS at a given constant bottom hole pressure

(BHP). He concluded that for gas-condensate LRS reservoirs, we have an equal amount of a producing OGR to the solution OGR at a specific BHP.

It is very important to make an accurate recombination of the producing OGR for better and correct well predictions. The main interest of this study is to make some investigation whether the producing OGR could be higher or lower that the solution OGR under a given specific analysing conditions. As many studies conclude it is very common to observe a producing GOR generally exceeding the initial GOR in an oil reservoir when the reservoir pressure around the wellbore drops below the bubble point pressure. Gas come out of the solution, it is much more mobile and this is reflected as an increase in GOR. It is also possible to get a producing OGR in gas-condensate greater than the initial or solution OGR at a constant rate. This can be observed in a highly fractured rich gas-condensate reservoir with a bed dip of about 24 degrees. Gravity played a major role here. Initially the reservoir pressure was greater than the saturation pressure so the producing OGR was as equal as the initial OGR. Later with the pressure below the saturation pressure, condensate accumulated in the formation, it flows to the base of the structure through the fractures and so the OGR increased at the down-dip producer. The gas rate at the surface decreases significantly at a later time because of the accumulation of liquid in the wellbore increased the well fluid density reducing rates.

However, in this study we are interested to do our investigation for oil reservoir, lean gas-condensate reservoir and liquid rich component gas-condensate reservoir under specific analysing conditions. The conditions to analyse are the infinite-acting period (boundary not reached) and well producing at a constant rate. Both compositional reservoir model and black oil model has been simulated and in both cases we have used a single-layer, two-dimensional and radial model. We have set the well at the centre of a cylindrical reservoir and for easier investigation parameters like skin-factor, capillary-force, gravity effects and non-Darcy effects have been neglected through out the entire study. We have performed simulations of an oil reservoir, lean-gas reservoir and rich gas-condensate reservoirs and we have investigated the behaviour of the producing OGR for the different reservoir

within the infinite-acting period and at a constant rate. We have started to simulate at an initial pressure equal to the saturation pressure (bubble point and dewpoint) within the infinite-acting period and producing with constant rates for a different choices of oil rates and gas rates respectively.

Chapter 2 explains some of the characteristics of the above-mentioned reservoir and their flow behaviours together with their fluid sampling procedures and PVT analysis. The proceeding chapters discusses the fluid sampling descriptions, main reasons for the GOR being constant at the infinite-acting period and the conditions and procedures for the fluid sampling to get the correct rate at which we can take our sample that represents the in-situ composition during the sampling.

Chapter 2.

2 .1 Theory

2.1.1 Flow behaviour of gas-condensate:

Fevang and Whitson (1995) have demonstrated the concept of phase flow regions for gas-condensate reservoirs near the well. The condensate starts to dropout cross the reservoir when the average pressure in a gas-condensate reservoir continues to decline on production.

→ **Region 1**: Outer part of the reservoir (inner near-wellbore) region where both liquid and gas flow simultaneously at different velocities. The reservoir pressure is greater than the dew point pressure.

$$\int_{P_{wf}}^{P^*} \left(\frac{K_{rg}}{B_{gd}\mu_g} + \frac{K_{ro}}{B_o\mu_o} R_s \right) d_p. \tag{2.1}$$

→ **Region 2**: The reservoir pressure is lower than the dew point pressure and is a region of condensate buildup where only gas is flowing. It is the middle part of the reservoir and the liquid starts to dropout in this region where as the condensate stays immobile.

$$\int_{P^*}^{P_d} \left(\frac{K_{rg}}{B_{gd}\mu_g} \right) d_p. \tag{2.2}$$

→ **Region 3:** The inner part reservoir (farthest away from well) and the pressure in the reservoir drops far below the dew point pressure. The accumulated condensate saturation goes above critical condensate saturation; both gas and condensate flow in this region and the pressure in this region drops at a very rapid rate.

$$K_{rg}(S_{wi}) \int_{P_d}^{P_R} \left(\frac{1}{B_{gd}\mu_g} \right) d_p. \tag{2.3}$$

The three flow regions are described in detail in figure 2.1 below by showing on pressure vs distance.

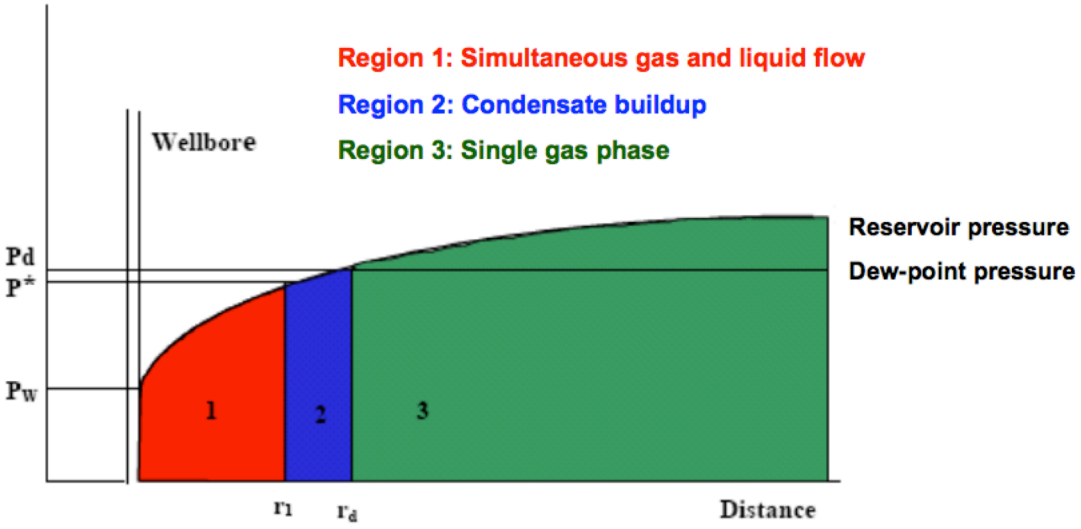

Figure: 2.1 gas-condensate flow behaviour

Table 1 below shows some of the typical characteristics of condensate, volatile oil and black oil from CNPC report, (2001). As we can see on the given data below, the volatile oil has a higher C7+ mole concentration compared to the C7+ of condensate near critical region.

Table 1: several fluids and their compositions (CNPC report, 2001)

	Condensate	Volatile oil	Black oil
CO_2 (mol%)	0.53 - 1.94	0.29	0.3
C_1 (mol%)	67.96 - 78.97	51.97	41.3
C_2 (mol%)	6.21 - 6.61	11.72	1.93
C_3 (mol%)	2.37 - 3.22	9.23	3.85
C_4 (mol%)	2.07 - 2.03	4.13	3.67
C_5 (mol%)	1.21 - 1.17	1.82	2.36
C_6 (mol%)	1.47 - 9.92	1.59	3.01
C_7 (mol%)	7.88 - 5.34	17.7	40.58
Mc_{7+}	135-145	185	228
γ_{c7+}	0.7925-0.7734	0.8231	0.8633
$T_{Res}(^0C)$	96.67-102.78	71.67	75.55
P_{sat}(Mpa)	30.5-36.5	28.1	19.7
$\rho_{liq}(g/cm^3)$	0.2867-0.3668	0.565	

A more quantitative hydrocarbon (HC) classification is shown on the ternary diagram below (SPE monograph v.20).

The ternary diagram below on figure 2.2 explains the different classifications of HC that are listed on table 1 above.

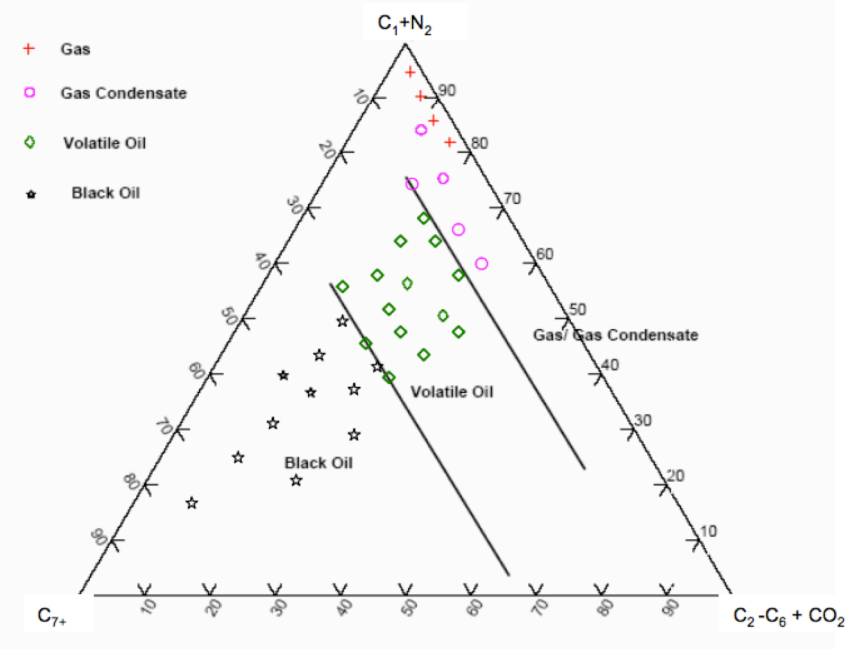

Figure: 2.2 Ternary classification of HC (SPE monograph, v.20)

2.1.2 Condensate Blockage:

Condensate blockage of gas-condensate wells is widely addressed as an important issue. In dry-gas wells, the blockage region is simply quantified by skin factor by interpreting pressure-transient testing outputs. In gas-condensate reservoirs, on the other hand the complex behaviour of gas-condensate fluids make difficulties for application of commonly used interpretation technique for estimating condensate skin. Chunmei Shi (2009) has described the concept of condensate blockage in the sense that when the reservoir pressure drops below the dew point, there is high tendency of condensate banking formation (condensate blockage effect) due to the pressure-drop occurring during production. Condensate blockage near the well may

cause a significant loss in well productivity for low-to-moderate permeability condensate reservoirs considering the main source for pressure loss in the tight reservoirs depend mainly on reservoir permeability. Fevang and Whitson (1996) performed their observation on their gas condensate reservoir modelling that the impairment of the well deliverability resulting from the near wellbore condensate blockage effect depends on the phase behaviour, absolute and relative permeability and the way the well is being produced. Fevang (1996) explained the dependency of well deliverability impairment, which is resulted from the near-wellbore condensate blockage on relative permeability and it applies mainly for gas and oil relative permeability ratios, which are on the ranges from 0.05 to 0.3.

As most compositional modelling presented that the saturation of condensate near the wells increases to approximately 68% while decreasing gas permeability and as a result gas productivity. When the reservoir pressure drops below the dew point the liquid starts to drop out and the gas moving towards wellbore is leaner with less condensate to drop out in the near wellbore region, consequently the condensate saturation decreases to about 55% and increases gas productivity. When the near wellbore gas mobility increased then the condensate blockage decreased.

Note: Curtis Whitson (2002) describes that the condensate blockage is very important if the pressure drop from the reservoir to the wellbore is a significant percentage of the total pressure drop from reservoir to deliverability point during and after a well goes on decline!

2.2 Fluid sampling procedure:

Taking representative reservoir fluid samples has become significant development and exploration of gas condensate reservoirs. There are several gas-condensate sampling methods however it is desirable to select a method that ensures continues representative sample of the well stream. Among the several gas-condensate fields located in the Norwegian North Sea, Sleipner, Trym and Atla are some of the typical fields. Fluid samples from gas-condensate reservoir are mostly taken by sampling the gas and liquid from the separator and recombining the samples at the producing

gas/liquid ratio. Thus, several simulation efforts has been made for gas condensate recombination process based on the matching of initial gas condensate dew point pressure with dew point of the recombined sample. It is very important to have a stable liquid and gas production rates and stable wellhead pressure before and during sampling. The best samples will be taken at a stable condensate gas ratio (CGR) where the rate is very low but is strongly suggested to take duplicate sets at different rates as well. McCain Jr and Alexander (1992) took three retrograde gas condensates with different compositions and they have investigated that the richest gases caused the largest build-up condensate around the wellbore. Their examinations were based on different initial reservoir pressures and dew point pressures of the original reservoir.

Johannes Bon and Hemanta Sarma (2007) recommended surface sampling through a stable separator as the best sampling method for condensate reservoirs. Their suggestion was based on the retrograde liquid drop down concept; the liquid will initially accumulate near the wellbore but ultimately with the continuous flow of fluids through the pore space the fluid mobilizes and its production results in a constant condensate gas ratio (CGR).

2.2.1 Surface Sampling methods:

Representative fluid samples can normally be obtained from producing reservoirs at surface conditions. However, in gas condensate reservoirs the properties of surface gas is different from the properties of reservoir gas. Sampling condensate reservoirs mainly involves sampling individual liquid and gas streams from a production separator and is by far the most common condensate sampling technique. The liquid condenses from the reservoir gas as it moves from the reservoir condition to the surface condition.

i) *Separator sample* is from test or production separator and mainly recommended for condensate reservoirs but it is also suitable for volatile-oil reservoir fluids. In order to take a representative sample we

simply recombine the stable separator liquid and gas in their produced ratio. Johannes Bon and Hemanta Sarma (2007) suggested that it is better to flow the well through the separator at a stable GOR, pressure and temperature for two or three separator volumes to ensure that the fluid that is collected in the separator any other points in the equilibrium state is flushed out.

- The most common separator sampling techniques are described as (in API):
- Filling an evacuated container
- Filling a piston like container

ii) *Wellhead sample,* is commonly used for under saturated that are on the single phase at wellhead conditions. This sampling can only be performed if the reservoir-fluid saturation pressure is certainly smaller less than the wellhead temperature and pressure.

iii) *Pipeline or plant flow line sample*, in this case it is significant to ensure that the fluid obtained is somehow close to the fluid, which was initially discovered in the reservoir, thus ensuring that it is a good representative sample.

2.2.2 Pressure test analysis (PTA):

The pressure transient analysis in gas-condensate reservoirs is way different from the other reservoir types and is very complicated due to the processes occurring in the near-wellbore region and especially saturation and compositional changes. Igder and Hashemi (2012) have made their pressure-transient studies based on the data obtained from an actual production well in a gas-condensate reservoir located south of Iran.

Identifying well behaviours and estimations of reservoir flow parameters has been well performed in several studies through pressure transient analysis (PTA) of

bottom-hole pressure data (BHP). However, in some situation where we have high temperature and high-pressure reservoirs (HPHT), permanent recording of bottom-hole data may not be always operationally possible. On the other hand wellhead (WH) pressure are available on most wells and they are continuously recorded by operating industries. It actually is more advantageous to gather information from WH data, since the cost of recording WH data is lower than that of a downhole survey and risks with regard to the running tools in the wellbore are eliminated. For gas-condensate reservoirs, the equation governing pressure transmission in porous medium is not liner. Al Hussainy and Ramey and Al Hussainy et al showed that the flow equation for real gases in porous media could be linearized using the real gas pseudopressure (single-phase pesudopressure equation):

$$m(p) = 2\int_{P_0}^{P} \frac{P}{\mu z} dp. \qquad (2.4)$$

The above equation (eq 2.4) is more suitable for dry-gas reservoirs and can be applied to gas-condensate wells that are producing above the dew-point pressure. But when the pressure falls below the dew point pressure and condensate bank starts to form around the wellbore then the single-phase equation will not be applicable anymore. The numerical experiments made by Shaosong Xu and W.John Lee (1999) explained that during reservoir depletion, the vapour properties *ín sítu* are a function of pressure only and correlates very well with z factor, viscosity and gas molar density obtained in lab constant composition expansion (CCE). In their experiment they have discussed the dependency of condensate PVT properties *ín sítu* on pressure, production mode and reservoir properties but the effect of variables other than pressure are very small and they are constrained within a certain pressure range. Henderson G. D., Danesh A., Tehrani D. H. and Peden J. M have shown the evaluation of the three-zone pseudopressure flow models with an integral as shown below:

$$m^{3zones}(P) = Zone1 + Zone2 + Zone3$$

$$m^{3zones}(P) = \int_{P_{wf}}^{P^*} \left(\frac{K_{ro}\rho_0}{\mu_0} + \frac{K_{rg}\rho_g}{\mu_g}\right) dp + \int_{P^*}^{P_{dew}} \left(\frac{K_{rg}\rho_g}{\mu_g}\right) dp \quad (2.5)$$

$$+K_{rg}(S_{wi}) \int_{P_{dew}}^{P_r} \left(\frac{\rho_g}{\mu_g}\right) dp.$$

2.3 Gas-condensate PVT analyses:

The standard experimental programs that we normally use for gas-condensate fluid involves: (1) recombined well-stream compositional analysis through C_{7+}, (2) CVD and (3) CCE. The CCE and CVD data are measured in a high-pressure visual cell in situations where the dew point pressure is figured out visually.

i) Constant Volume Depletion (CVD)

To quantify recoveries of gas-condensate reservoirs as functions of pressure below the dew point the outcomes from laboratory experiments can directly be employed because CVD test simulates directly the actual characteristic of gas-reservoir, which is undergoing pressure depletion as shown in figure 2.3. Here, the overall composition varies during the procedure. One thing that needs to be noticed in CVD test is that the condensate is assumed to be immobile. One can predict a complete a full depletion behavior during the entire period between the initial pressure and abandonment by combining it with the z-factor of a single-phase from CCE test.

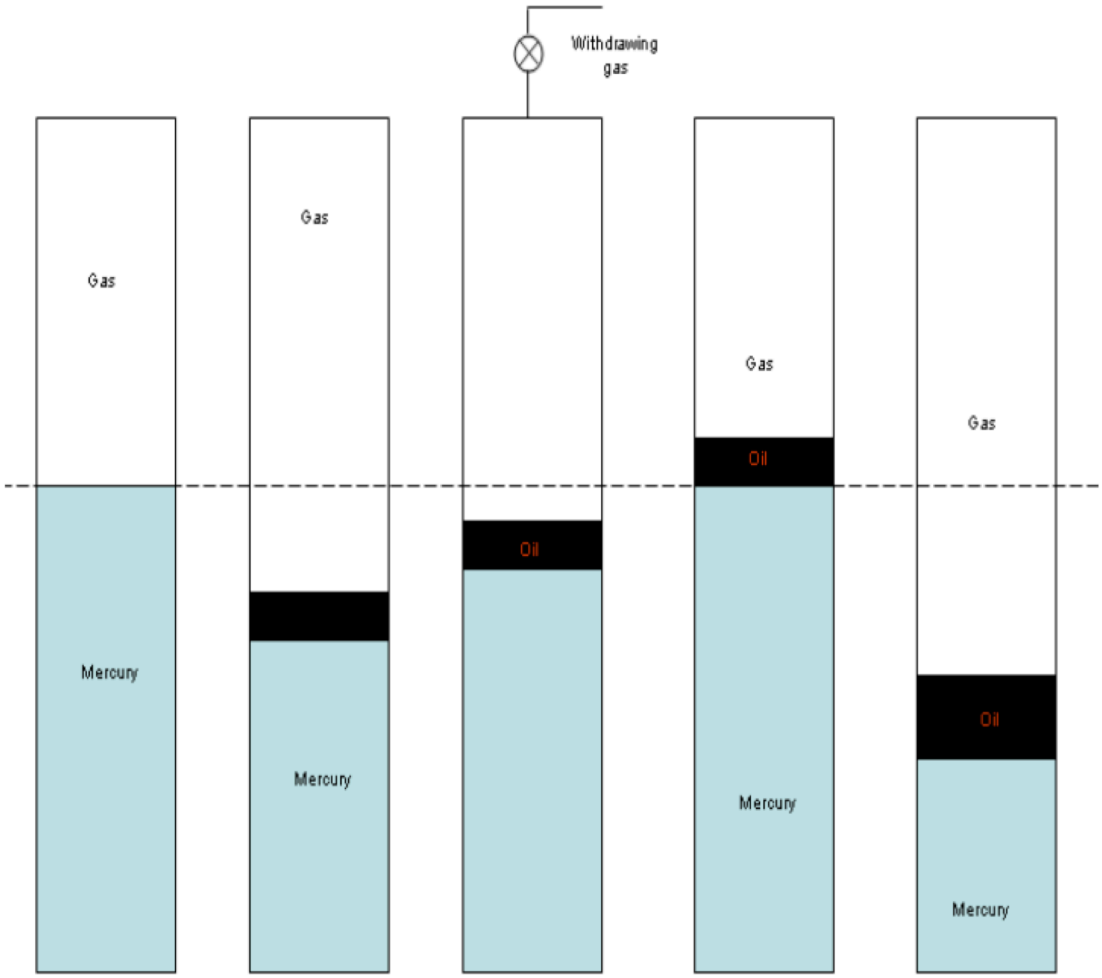

Figure 2.3: Schematic of CVD test (Vo 2010)

i) Constant Composition Expansion (CCE)

CCE is an important laboratory test and is able to simulate closely the actual behavior of a gas-condensate reservoir and is also knows as Constant Mass

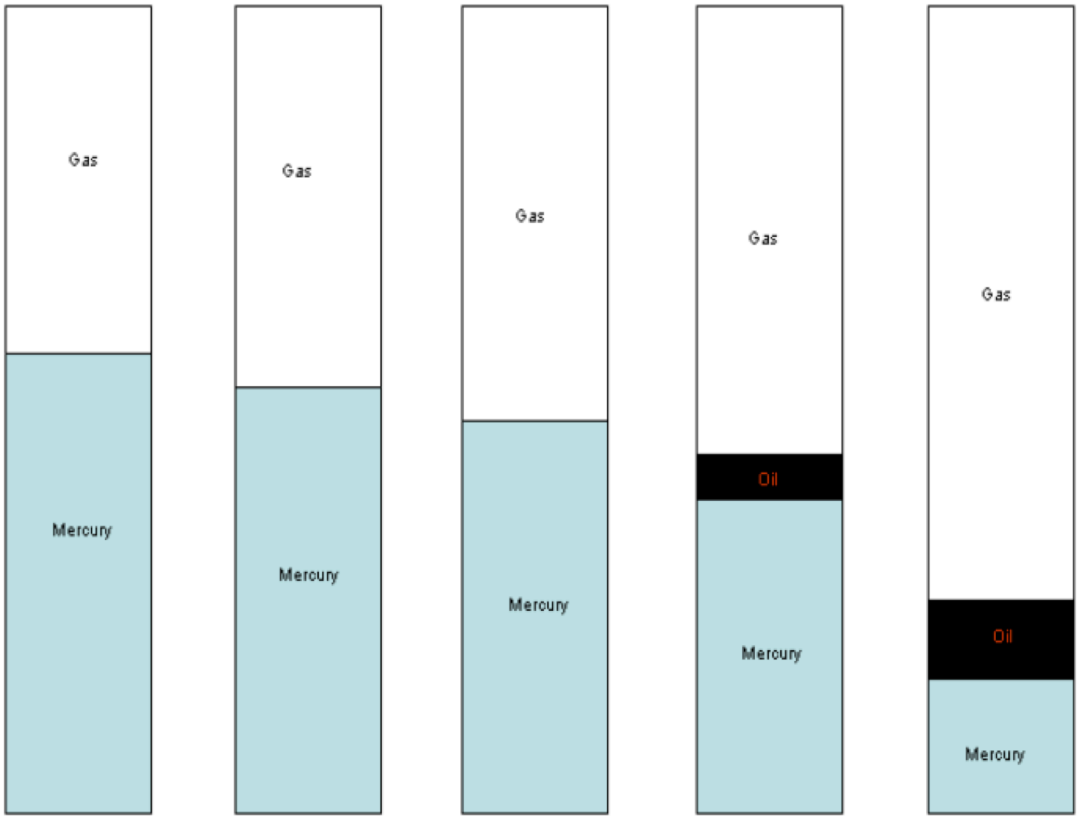

Figure 2.4: Schematic of CCE test (Vo 2010)

Expansion. The schematic of CCE is shown in the figure below figure 2.4.

2.4 Transient flow period

The transient condition is only valued for a relatively short period after some pressure disturbance has been created in the reservoir. As we can see from the figure below, at early times after a well has been out on production and at early time after a well has been shut in, flow occurs in a transient mode. In practical manner, if the pressure at the wellbore decreases, the reservoir fluids will start to flow near

the vicinity of the well. In radial flow model, the pressure disturbance would definitely be as a consequence of the alteration of the well's production rate at $r = r_w$. The material-balance (continuity) has to be considered when representing the transient flow period mathematically as shown in the equation below (diffusivity equation in radial coordinates).

$$\frac{1}{r}\frac{\partial}{\partial r}\left(r\frac{\partial P}{\partial r}\right) = \frac{\emptyset \mu c_t}{k}\frac{\partial P}{\partial t}. \qquad (2.6)$$

The expanding fluid's pressure drop will provoke flow from further, undisturbed reservoir region. (L.P. Dake) mentioned that the pressure disturbance and the movement of the fluid will continue its propagation radially away from the wellbore. During the time in which the transient flow condition is useable, it is considered that the pressure response in the reservoir is not influenced by the presence of the outer boundary, $i.e$, the reservoir exists infinite in extent. It is very important to be able to distinguish the different time conditions when we work with the above equation

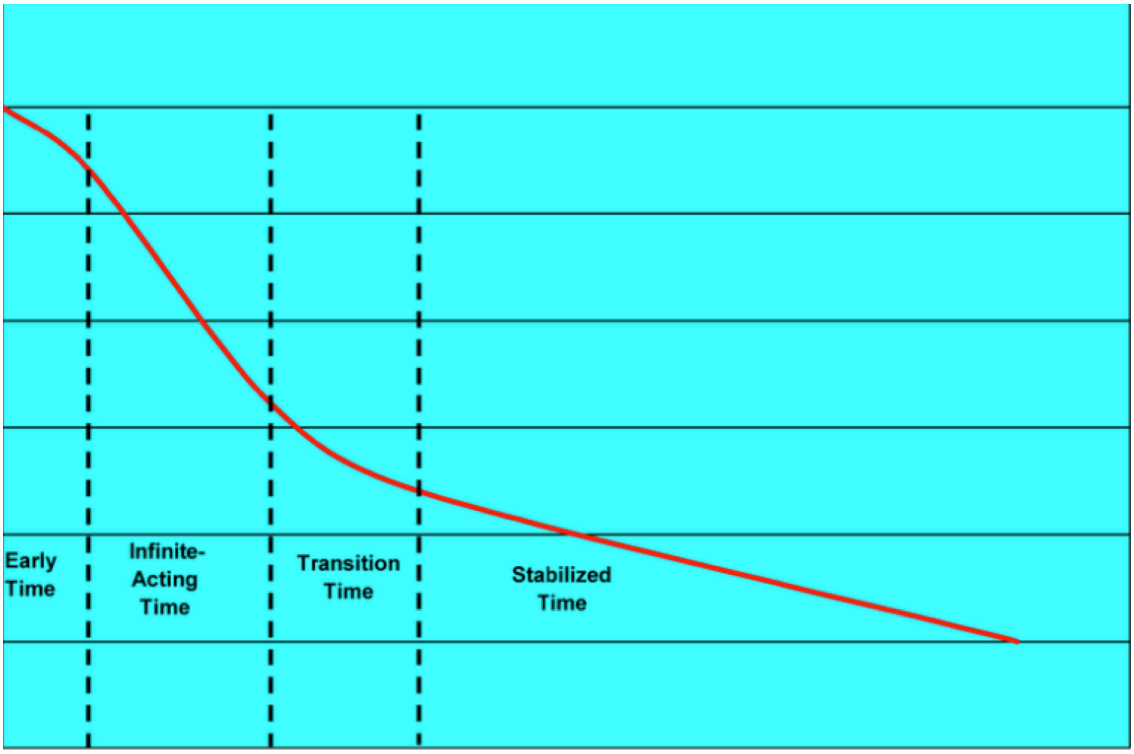

Figure 2.5: the resulting decline in bottom hole flowing pressure

(2.6) before an actual simulation work. In this paper we put more focus in the infinite-acting period. During the infinite-acting time, the well response is the same as the well being produced from an infinite reservoir. The resulting decline in BHFP is shown in figure 2.5 below.

2.4.1 Infinite acting period

The concept of infinite acting period has been discussed in various literatures and in several cases. A well that is set at a constant flow rate of production after a shut-in period starts to show a pressure disturbance spread in the reservoir when the pressure in the wellbore starts to drop. There is no any effect to the rate at which the pressure disturbance spreads in the formation, either by the shape of the drainage area or any influences of the reservoir boundaries. Due to such reasons the transient state flow period is also know as the infinite acting state. The figure below shows the schematics of the pressure distribution development where the production well creates an expanding pressure sink at the inflow face. It shows that the slope of the pressure sink at the inflow face is constant as long as the production happens at a constant rate. At the infinite acting period the pressure distribution through the reservoir and the decline rate of the wellbore are determined by the reservoir and fluid characteristics like permeability, porosity, viscosity and total compressibility. The term constant terminal rate solution describes the equation of P_{wf} versus time (t) at constant production rate for different values of the time flow. The pressure decline curve can mostly be divided into three sections depending on the geometry of the reservoir (in our case circular) and the value of the flowing time. The schematically pressure distribution results shows the three different flow periods: 1) the first period where the outer boundary is not yet felt and is called the infinite-acting period, it is assumed that the drainage boundary of the well is not affected by the pressure response at the wellbore and vice versa. 2) The second period known as the transition period, which is in the middle, and 3) the third period called the late-time period where a steady shape exists. In this late period, the pressure profile normally shows a steady shape and due to that reason that

period is called the semi steady-state period. In cases of infinite acting reservoirs($r_{eD} = \infty$), the dimensionless pressure drop P_D becomes a function of the dimensionless time t_D that is:

$$P_D = f(t_D). \tag{2.7}$$

The dimensionless time t_D can be formulated as:

$$t_D = \frac{0.000264kt}{\emptyset(c_t\mu)_i r_w^2}.$$

In the first period, the reservoir characterises as if in an infinite extent during the first period and is called as infinite-acting period. Carlslaw, H.S. and Jaeger, J.A showed the pressure distribution during the infinite-acting period as follows:

$$P_i - P = \frac{2u_{sc}(\mu B)_r}{k}\left[\sqrt{D_h\, t/\pi}\, exp\left(\frac{-x^2}{4D_h t}\right) - \frac{x}{2} erfc\, \frac{x}{2\sqrt{(D_h t)}}\right]. \tag{2.8}$$

$$P_i - P = \frac{2u_{sc}(\mu B)_r}{k}\sqrt{D_h t}\;\; ierfc\frac{x}{2\sqrt{(D_h t)}}\;.$$

Where $erfc =$ the complementary error function defined by

$$erfc(y) = 1 - \text{erf}(y) = 1 - \frac{2}{\sqrt{\pi}}\int_0^y exp(-u^2)\, du.$$

$ierfc =$ The integral of erfc defined by

$$ierfc(y) = \int_y^\infty erfc(x)dx\,.$$

The mathematical solution for the infinite-acting period comes from the diffusivity equation (2.6), expressed with the dimensionless variables as

$$r_D = \frac{r}{r_w} \quad and \quad t_D = \frac{kt}{\emptyset\mu c_t r_w^2}.$$

$$P_D = \frac{kh\Delta P}{q_{sc}\beta}. \tag{2.9}$$

Where,

$\beta = \frac{\overline{B_g}\overline{\mu_g}}{2\pi}$ $\quad and \quad \Delta P = P_i - P(r,t).$

The infinite-acting period in field units can be determined as:

$$t_{eia} = \frac{\emptyset(\mu c_t)_i A}{0.000264k} * (t_{DA})_{eia}. \tag{2.10}$$

Since we have a cylindrical (circular) reservoir, we will consider $(t_{DA})_{eia} = 0.1$ in our case through out the entire discussion.

L.P.Dake has explained the pseudo-pressure vs distance on figure 2.6 at a various and specific time.

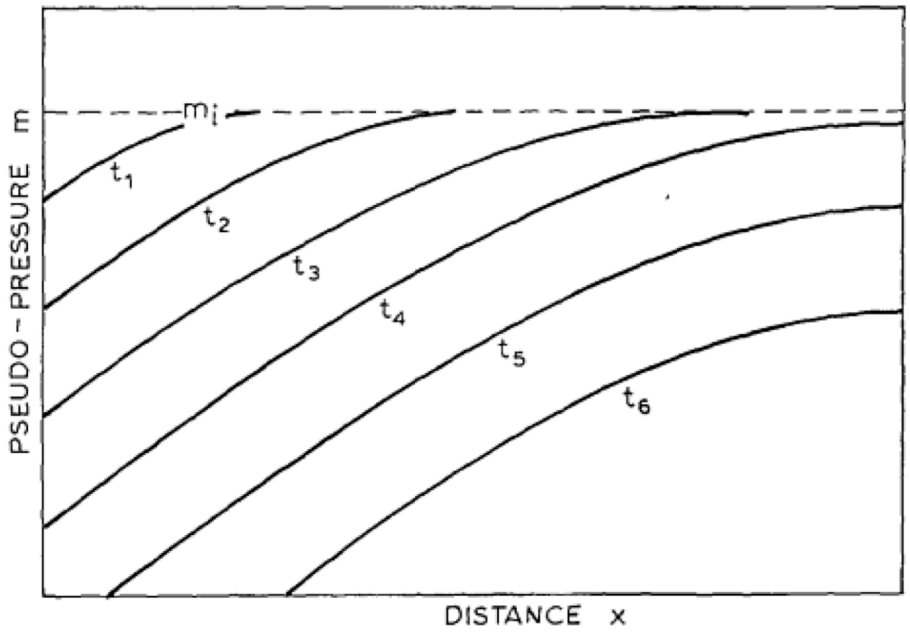

Figure 2.6: Pseudo-Pressure distribution at a constant rate (L.P. Dake)

2.4.2 Radius of investigation:

The radius of investigation (r_{inv}) in the figure indicates the distance or the extent at which the transient effect have travelled into the reservoir. When change in rate occurs at the well then pressure transient starts to be created and advances further more into the reservoir with time. This radius of investigation which is shown in figure 2.7 below is created by the producing well is a function of time. Energy Recourses Conservation Board ERCB (1975) shows the analytical radius of investigation formula as follows:

$$r_{inv} = \sqrt{\frac{kt}{948*\emptyset*\mu*C_t}}. \tag{2.11}$$

But for practical purposes, it is more convenient to use radius of investigation:

$$r_{inv} = 2\sqrt{t_D r_w^2}\,. \tag{2.12}$$

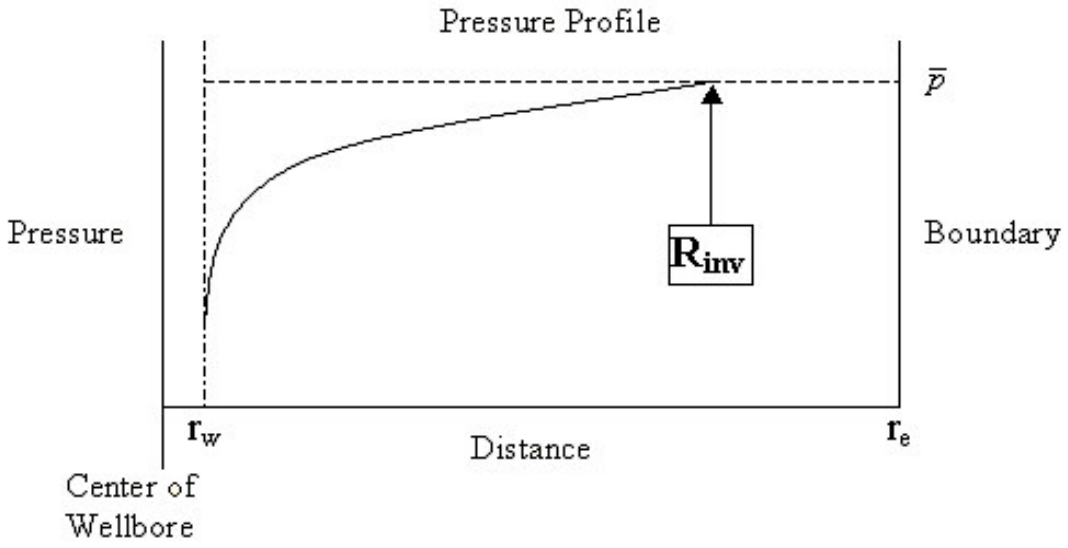

Figure 2.7: Illustration for radius of investigation

The above diagram illustrates the basic concept of radius of investigation by applying pressure versus the distance into the reservoir. The radius of investigation does not depend on the flow rate but it is highly dependent and function of the reservoir properties. Any changes in the flow rate will not show any effects on the radius of investigation however an increase in flow rate will tend to give a greater drawdown $(\bar{P} - P_{wf})$.

2.5 Conditions for the test

During the simulations, various conditions had been performed to test the resulting OGR, and some of them are changing initial pressure or the distance between the initial pressure and the dewpoint pressure, having low permeability reservoir and several PVT data that are richer in liquid components. In addition, adjusting $i.e$ increasing the grid block size and decreasing the simulation time step has been an important trail.

2.5.1 Effects of low permeability in the reservoir

Zhang and Wheaton (2000) have discussed the effects of low permeability and reservoir heterogeneity on condensate banking in terms of condensate to gas ratio. It has also been mentioned the possible events where the low permeability region of the reservoir intersperses the high permeability region of the reservoir. Cutris Whitson and Fevang (2002) performed the problems related to the modelling and experimental design of relative permeability used for simulating gas condensate well deliverability. In gas condensate wells the relative permeability k_{rg}, as a function of k_{rg}/k_{ro} is the main parameter that defines the steady-state flow and a more generalized model is developed for a relative permeability as a function of k_{rg}/k_{ro}.

Curtis Whiton (2012) made a case study on liquid rich shale (LRS) and discussed that the reason behind low producing oil gas ratio (OGR) is as a result of very low permeability which ultimately lead to large drawdowns and fluid flow with localized and large gas-to-oil mobility ratio gradients near the fracture. The study showed that the liquid yield remains constant from the initial testing stage throughout the entire life of the well. He mentioned that for a constant production rate, the drawdown would be higher causing an increased liquid dropout around the well.

2.5.2 Liquid gas ratio (LGR):

A gas-condensate reservoir can be choke or come out on its most valuable components. The saturation of liquid condensate can build up near the well due to the drawdown below the dew point pressure, which eventually restricts the flow of gas. Wheaton and Zhang (2000) have developed the theoretical treatment of condensate banking dynamics and they have shown how the composition of heavy components of a gas-condensate change with time around production wells during depletion. They have pursed some numerical simulations to confirm and supplement their theoretical analysis and they have interpreted liquid gas ratio with developed analytical model. The effect of low permeability and reservoir

heterogeneity on condensate banking in terms of condensate to gas ratio has also been performed. The sub-sections below will demonstrate the sensitivity of liquid gas ratio at varying conditions, example: the effect of liquid gas ratio with respect to rate and distance between initial pressure and dew point.

The proceeding chapters will demonstrate and explain the detailed OGR results and the different simulation that has performed for both the compositional and blackoil models. The fluid sampling conditions and procedures will be discussed in details at an infinite-acting period with high drawdown.

Chapter 3

3 Reservoir Modeling and Simulations

This section describes and shows a system that allows us to monitor and control a reservoir simulation run. The different output of our simulation for all the reservoirs mentioned earlier will be discussed here in details and over all the producing OGR with respect to the solution OGR will be our main focus through out this entire section. The simulated reservoirs are model as radial, 2D, single-layer and homegenous reservoirs under the analysing conditions of infinite-acting period and constant production rate. The models are simulated on Eclipse E300 (condensates) and E100 (Blackoil) that is commercially availabe multitasking software. The non-Darcy effects, gravity effects, capillary forces and skin factor are

Table 2: The reservoir properties that are applied both in the Compositional and Blackoil simulations.

Parameters	Lean gas-Condensate	Rich gas-condensate
Reservoir Porosity ∅, %	20	30
Absolute permeability (horizontal) k, mD	5	6
Well radius r_w,	0.10 m	0.35 ft
Irreducible water saturation S_{wi}, %	0	25
Reservoir thickness h,	25 m	200 ft
Rock compressibility,	$5.075 * 10^{-5}$ $bars^{-1}$	$5.00 * 10^{-6}$ $psia^{-1}$
Skin factore, S	0	0
Reservoir drainage area,	$2.626 * 10^6 m^2$	650 acres
Reservoir temperature T_{res},	110 C^0	266 F^0
Initial reservoir pressure P_{res},	425 bars	6500 psia
Total reservoir radius r_e,	914.2 m	3000 ft
Relative permeability at S_{wi},		0.8
Water compressibility,		$2.67 * 10^{-6}$ $psia^{-1}$
Minimum BHFP P_{wfmin},	68 bars	1500 psia
Saturation pressure,	417.05 bars	5900 psia

neglected and the reservoir models have 30 grid blocks increasing logarithmically with radius away from the wellbore. Lean gas-condensate, rich gas-condensate and blackoil reservoir properties and their radial grid block distributions are shown below in table 2 and table 3 respectively.

Table 3: radial grid size distribution of the 2D for lean gas-condensate

Inner most Grid radius, [m]	0.20
Reservoir grid cell size in radial direction, [m]	0.2512 0.3155 0.3963 0.4977 0.6252 0.7852 0.9862 1.2387 1.5558 1.9541 2.4544 3.0827 3.8719 4.8631 6.1081 7.6718 9.6358 12.1026 15.2009 19.0924 23.9802 30.1192 37.8299 47.5146 59.6786 74.9567 94.1460 118.2479 148.5200 186.5419

Table 4: radial grid size distribution of the 2D for rich gas-condensate

Inner most Grid radius, [m]	0.35
Reservoir grid cell size in radial direction, [m]	0.53 0.89 1.39 2.15 3.35 5.20 8.07 12.5 19.46 30.23 36.94 72.9 113.2 175.01 273.01 423.97 658.41 1022.49 1587.88 2465.9

Single-phase Pseudo-pressure

(Al Hussainy & Ramey) the diffusivity equation of gas can simply be described in a linearized form by a single-phase Pseudo-pressure function, named as real gas potential. Knowing gas is the dominant fluid in gas-condensate reservoirs, the single-phase Pseudo-pressure is employed:

$$m(P) = 2\int_{P_{wf}}^{P} \frac{P}{\mu(P)Z(P)}dP. \tag{3.1}$$

$$m(P) = 2\int_{0}^{P} \frac{P}{\mu_g Z}dP - 2\int_{0}^{P_{wf}} \frac{P}{\mu_g Z}dP. \tag{3.2}$$

Where μ *and* Z are the viscousity and compressibility factor of the real gas consecetively. We obtain the slope (m) of the semilog plot of m(P) versus log of the time from (3.1). The values of all the parameters in (3.1) were taken from s CVD simulation of PVTsim.

$$m(P) = \sum \frac{\overline{2P}}{\mu Z} \cdot \Delta P \left(\frac{Psia^2}{cP}\right)$$

Figure 3.1 below explans the m(p) vs pressure corresponding the parameters given in table 5.

Table 5: Trapezoidal rule used for the determination of the real gas Pseudo-Pressure which is a function of real pressure.

P(Psia)	Z_g	μ_g	$\frac{2P}{\mu Z}$	$\frac{\overline{2P}}{\mu Z}$	ΔP	$\frac{\overline{2P}}{\mu Z} \cdot \Delta P$	$m(P) = \sum \frac{\overline{2P}}{\mu Z} \cdot \Delta P \left(\frac{Psia^2}{cP}\right)$
400	0.957	0.01312	63704.05649	31852.028	400	1.274E+07	1.2740E+07
800	0.932	0.01381	124290.1947	93997.126	400	3.760E+07	5.0339E+07
1200	0.912	0.01461	180162.1529	152226.174	400	6.089E+07	1.1123E+08
1600	0.897	0.01563	228267.2796	204214.716	400	8.169E+07	1.9292E+08
2000	0.887	0.01694	266195.189	247231.234	400	9.889E+07	2.9181E+08
2400	0.882	0.01858	292839.8274	279517.508	400	1.118E+08	4.0362E+08
2800	0.883	0.02058	308179.194	300509.511	400	1.202E+08	5.2382E+08
3200	0.889	0.02293	313910.6702	311044.932	400	1.244E+08	6.4824E+08
3600	0.901	0.02566	311452.0241	312681.347	400	1.251E+08	7.7331E+08
3400	0.918	0.02878	302756.8049	307104.414	400	1.228E+08	8.9615E+08
4400	0.942	0.03240	288337.2507	295547.028	400	1.182E+08	1.0144E+09
4800	0.972	0.03668	269291.5931	278814.422	400	1.115E+08	1.1259E+09
5200	1.012	0.04189	245351.2853	257321.439	400	1.029E+08	1.2288E+09
5600	1.062	0.04814	219059.7785	232205.532	400	9.288E+07	1.3217E+09
6000	1.119	0.05471	196029.7885	207544.783	400	8.302E+07	1.4047E+09
6074	1.13	0.05587	192422.4798	194226.134	74	1.430E+07	1.4190E+09
6400	1.17	0.05794	188820.9096	190621.695	326	6.221E+07	1.4812E+09
6800	1.218	0.06049	184579.7447	186700.327	400	7.468E+07	1.5559E+09
7200	1.266	0.06307	180352.5931	182466.169	400	7.299E+07	1.6289E+09
7600	1.314	0.06567	176155.4951	178254.044	400	7.130E+07	1.7002E+09
8000	1.362	0.06830	172002.2208	174078.858	400	6.963E+07	1.7698E+09
8400	1.41	0.07096	167905.4691	169953.845	400	6.798E+07	1.8378E+09
8800	1.457	0.07366	163988.1707	165946.820	400	6.638E+07	1.9042E+09
9200	1.505	0.07640	160027.8006	162007.986	400	6.480E+07	1.9690E+09
9600	1.552	0.07917	156251.047	158139.424	400	6.326E+07	2.0323E+09
10000	1.599	0.08199	152551.9992	154401.523	400	6.176E+07	2.0940E+09
10400	1.646	0.08485	148935.7055	150743.852	400	6.030E+07	2.1543E+09
10800	1.692	0.08774	145492.0594	147213.882	400	5.889E+07	2.2132E+09

11200	1.739	0.09068	142047.2756	143769.667	400	5.751E+07	2.2707E+09
11600	1.785	0.09366	138771.4671	140409.371	400	5.616E+07	2.3269E+09
12000	1.831	0.09668	135580.3728	137175.920	400	5.487E+07	2.3818E+09
12400	1.878	0.09974	132404.3743	133992.374	400	5.360E+07	2.4353E+09
12800	1.923	0.10283	129455.398	130929.886	400	5.237E+07	2.4877E+09
13200	1.969	0.10597	126521.6834	127988.541	400	5.120E+07	2.5389E+09
13600	2.015	0.10915	123672.9429	125097.313	400	5.004E+07	2.5890E+09
14000	2.061	0.11236	120908.2672	122290.605	400	4.892E+07	2.6379E+09
14400	2.106	0.11562	118282.4714	119595.369	400	4.784E+07	2.6857E+09
14800	2.151	0.11890	115733.1162	117007.794	400	4.680E+07	2.7325E+09
15200	2.197	0.12223	113207.3702	114470.243	400	4.579E+07	2.7783E+09
15600	2.242	0.12559	110808.9267	112008.148	400	4.480E+07	2.8231E+09

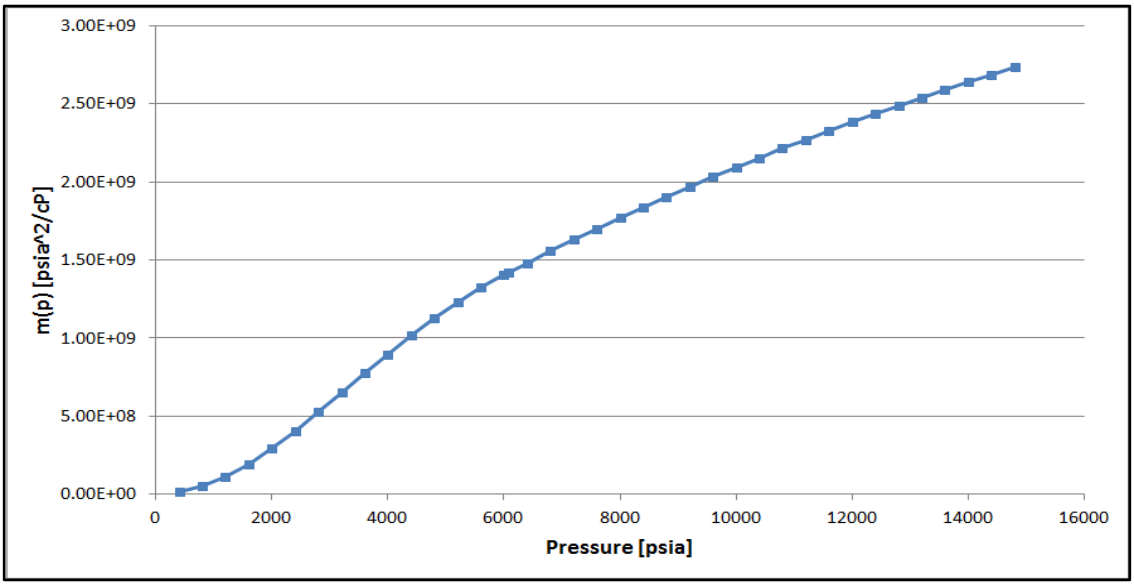

Figure 3.1: Curve showing the reltion between real gas Pseudo-pressure and real pressure.

3.1 Oil gas ratio (OGR)

Most studies showed that the pressure profile within the condensate bank changes with time during the pressure depletion. The pressure decreases at any point in the bank for a homogeneous reservoir. From the simulation (Eclipse-300), the effect of OGR with respect to the distance between initial pressure and dew point has been performed. It has been observed that as the initial pressure (distance from dew

point) increases then the OGR starts to increases, which ultimately approaches to the initial OGR keeping the rate constant.

3.1.1 Lean gas-condensate

Nowadays it is recognized that to secure greatest ultimate recovery of petroleum from a reservoir it is important to maintain at all times the highest possible ratio of oil to gas production. There are numerous methods of securing high ratios, however they are not generally understood or practiced. Among these different ways of achieving higher ratios, we have performed some experiments by increasing the distance between the dew point and the initial pressure at constant rates, lower permeability in the reservoir and other related studies. We have performed our studies by making simulations in a condensate reservoir with more rich in liquid components, which will be explained later in this section. The figures below show the effects of initial pressure on the OGR value by increasing the distance between the dew point and the initial pressure at a constant rate.

- The OGR value at a constant rate of $0.2 * 10^6\ SM^3/SM^3$ has been taken with varying the initial pressure fig 3.2. The producing OGR (r_p) tends to increase and get closer to the initial OGR value as the initial pressure kept increasing for some extent. With an initial pressure of 430 $bars$, the producing OGR (r_p) is about 6% lower than the initial OGR (r_i). Increasing the initial pressure by 10 $bars$ (440 $bars$) brought the producing OGR value to be closer to r_i with a difference of only 3% and eventually at an initial pressure of 460 $bars$ the producing OGR value will reach to the initial OGR value $i.e\ (r_p = r_i)$.

- According to the experiment, the producing OGR will require a higher initial pressure to reach the initial OGR level at a higher rate. The simulation performed at a surface gas rate of $20.0 * 10^6\ SM^3/SM^3$ that is shown in figure 3.3 below requires an initial pressure of up to more than 520 $bars$ to stabilize and get somewhere closer to the initial OGR value at the same simulation period.

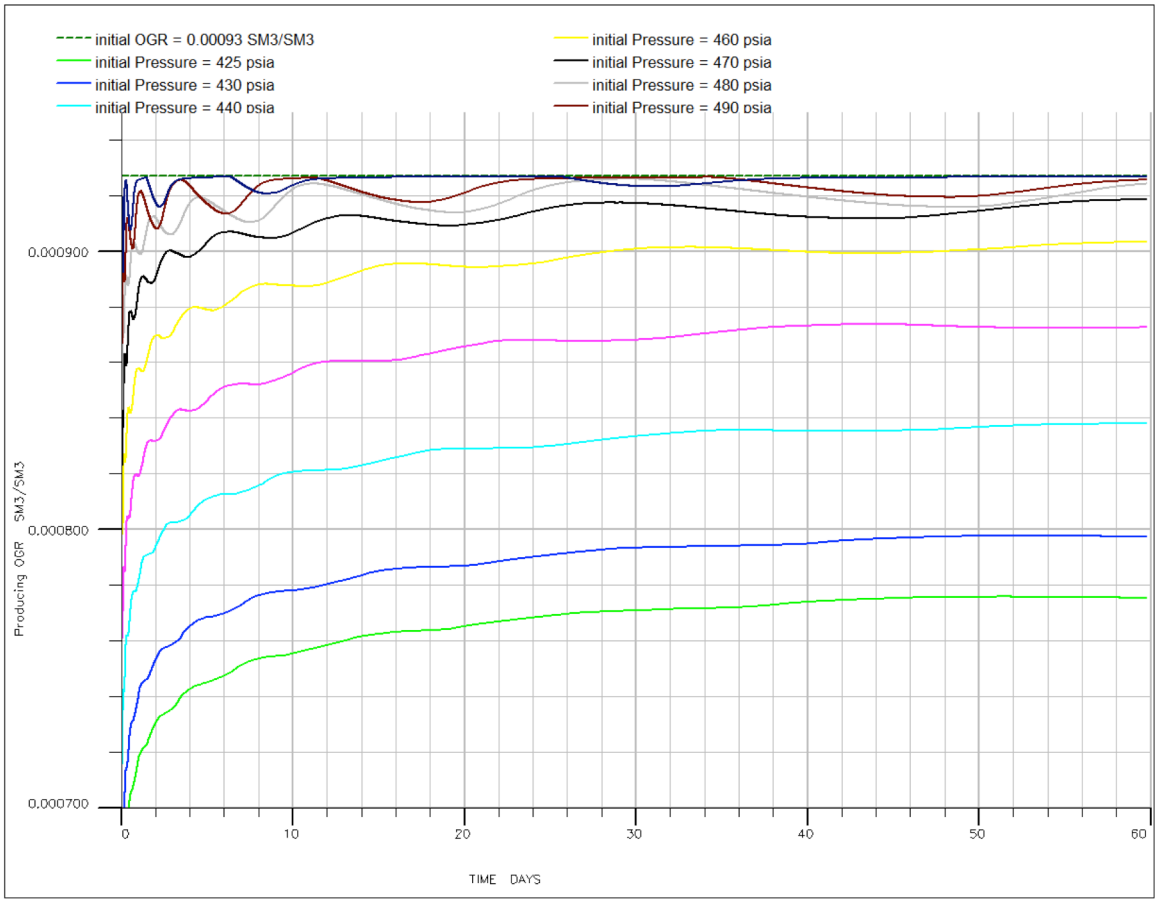

Figure 3.3: Producing OGR (r_p) behaviour with the corresponding initial pressure at a constant rate of $20 * 10^6\ SM^3/D$.

The simulations from the above figures (fig 3.1-2) indicates that at a constant rate the more distance between initial pressure and dew point pressure the more stable OGR results and depending on the amount of applied flow rate the producing OGR becomes equal to the initial OGR at a certain pressure. At a rate of 2.0E5 Sm^3/d the

producing OGR stabilizes and becomes equal with the initial oil-gas ratio value at a pressure of 471 bars ($r_i = r_p = 0.00093\ Sm^3/Sm^3$). However, the producing OGR value stabilizes at different initial pressures depending how large or small the flow rate is and it does not go above the initial oil-gas ratio once it reaches the initial OGR (maximum value). The higher the flow rate the higher initial pressure or the larger distance between dew point pressure and initial pressure requires for the producing OGR to stabilize and approach the initial OGR.

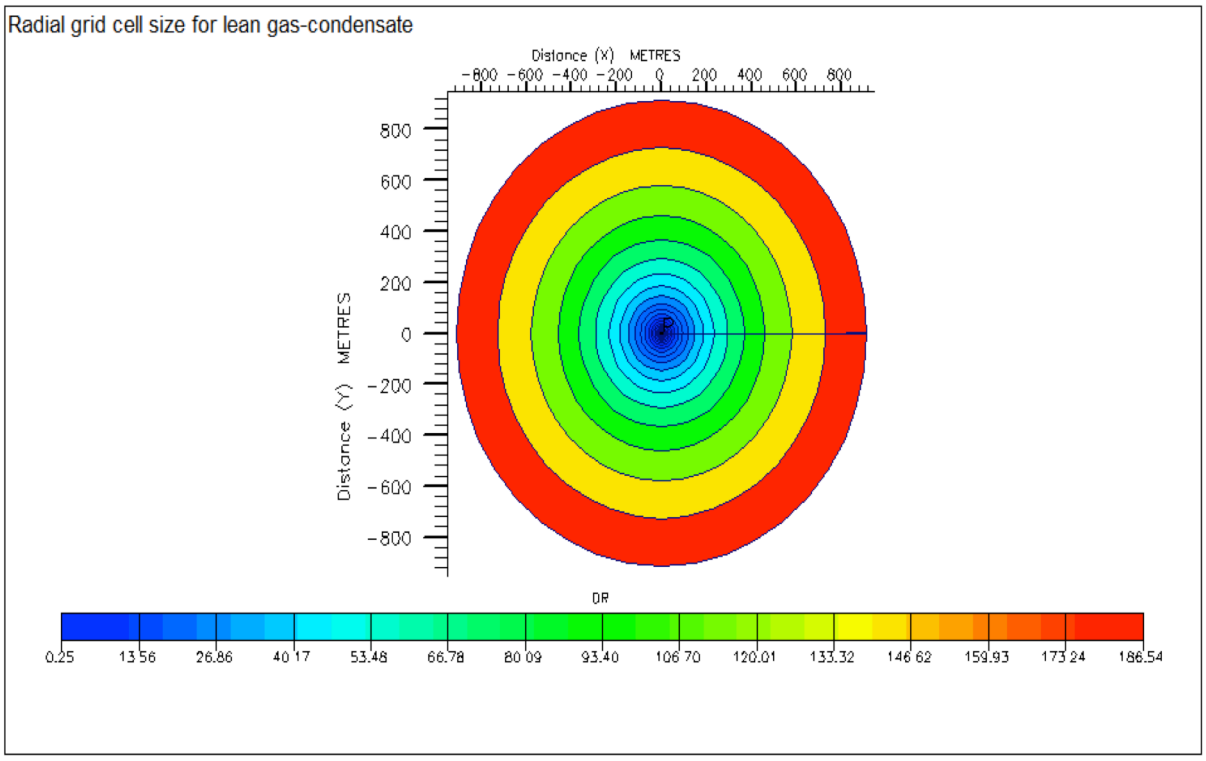

Figure 3.4: Top view of the 2D radial grid cell size for lean gas-condensate model.

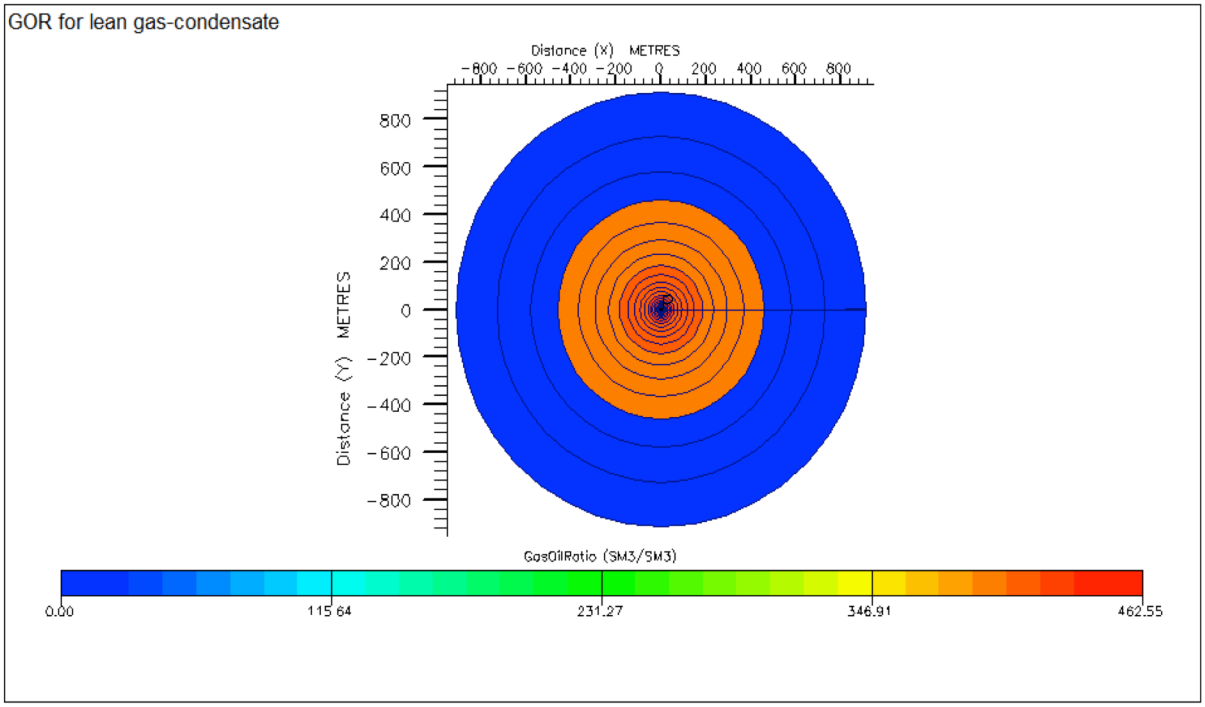

Figure 3.5: Top view of the 2D GOR distribution for lean gas-condensate model.

A detailed study for the behaviour of the producing oil-gas ratio corresponding the surface-gas rate has been made at two different cases:

- Initial pressure > Saturation pressure
- Initial pressure = dewpoint pressure

$Where, P_i = 425\ bars\ and\ P_d = 417.05 bars$

Figure 3.7 below shows the behaviour of the producing oil-gas ratio of a gas-condensate fluid below the saturation pressure at a given constant rate in the infinite-acting period. We have taken ten various constant rates at the infinite-acting period (in this case 60 days) where the limiting or minimum bottom hole pressure is set to be approximately 68 bars. As we can see in the last given three rates of $4.0E05\ SM^3/D$, $4.5E05\ SM^3/D$ and $5.0E05\ SM^3/D$ the flowing bottom hole pressure drops fast and shows a higher drawdown due to the decline in the flow rate once the pressure reaches the limiting BHP of 68 bars. However in the first seven given rates of $0.5E05\ SM^3/D$ to $3.5E05\ SM^3/D$, the producing OGR seems to show a sudden decrease but remains constant throughout the infinite-acting period.

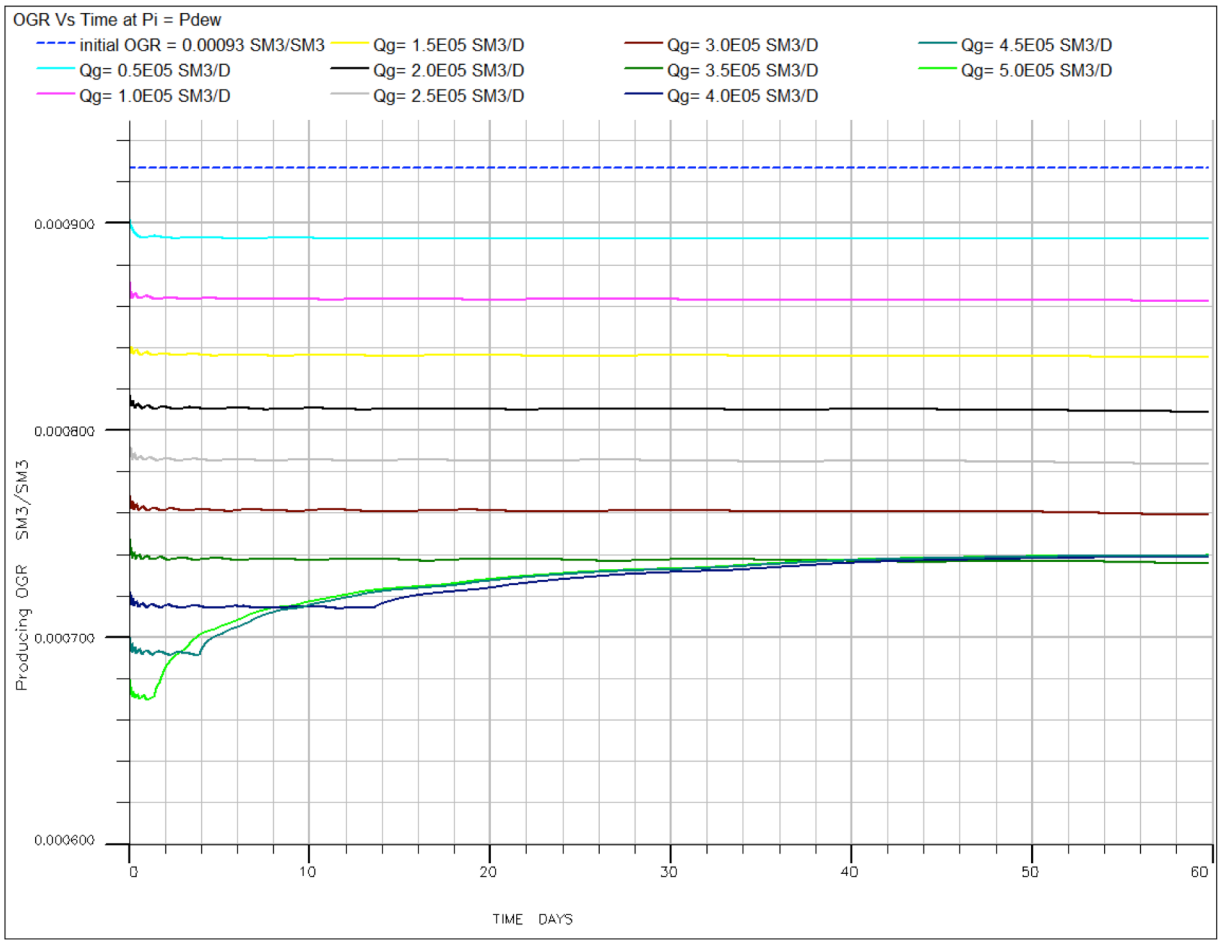

Figure 3.7: Producing OGR behaviour Vs time with corresponding constant surface-gas rate during a drawdown of vertical well where $\boldsymbol{P_i = P_d}$ in the infinite-acting period of radial, 2D and compositional gas condensate.

3.1.2 Comparison of the producing OGR

We have made some comparison between both the above cases $i.e$ for $P_i > P_d$ and $P_i = P_d$ at the same constant surface-gas rate to see the effect of the producing OGR, r_p relative to the solution OGR, r_i (see figure 3.8 below). From our simulations results we have concluded that, the producing OGR in the case where $P_i > P_d$ is higher than the producing OGR of case $P_i = P_d$ by about 3% for an equal amount of surface-gas rate. At a surface-gas rate of $0.5E05\ SM^3/D$ we have a producing OGR of

0.000926 SM^3/SM^3 at $P_i > P_d$ where as the producing OGR for the $P_i = P_d$ case drops to 0.00089 SM^3/SM^3.

3.2 Rich-gas condensate (radial well)

This section presents the observations of a field simulations for a rich gas-condensate reservoir with high drawdown with its composition listed in table 6. Several parameters $i.e$, reservoir properties, rock-fluid properties, geological, petrophysical and well data were used to construct the simulation model together with Equation-of-state and compositional model for the 15-components. The constructed simulation model was then used to make some investigations regarding the behaviours of rich gas-condensate reservoir within the infinite-acting period at a constant production rate where we could observe the results of the producing OGR.

On our earlier discussion of the flow regions in chapter-2 (section 2.1.1) the Psuedopressure calculations were shown. Fevang and Whitson (1995) have discussed the deliverability loss in region-1 due to condensate blockage by performing a primary functional relationship $k_{rg} = f(k_{rg}/k_{ro})$ for the rich gas-condensate that we have simulated. From the integral equations in section 2.1.1 if $P < P^*$ then we can find the PVT properties $R_s, B_o, \mu_o, \mu_g, B_{gd}\ and\ r_s$ directly as,

$$R_p = R_s + \left(\frac{k_{rg}}{k_{ro}}\right)\left(\frac{\mu_o B_o}{\mu_g B_{gd}}\right)(1 - r_s R_p). \tag{3.3}$$

We can simply use eq (3.3) to calculate the k_{rg}/k_{ro} as a function of pressure $i.e$

$$\frac{k_{rg}}{k_{ro}}(P) = \left(\frac{R_p - R_s}{1 - r_s R_p}\right)\frac{\mu_g B_{gd}}{\mu_o B_o}. \tag{3.4}$$

But (3.4) can be expressed in terms of the oil relative volume of the gas flowing in a period of constant composition expansion as

$$V_{roCCE} = \frac{V_o}{V_g + V_o}\ thus, \frac{k_g}{k_{ro}}(P) = \left(\frac{1}{V_{roCCE}} - 1\right)\frac{\mu_g}{\mu_o}. \tag{3.5}$$

For any producing OGR (r_p) the V_{roCCE} can be expressed from (3.2) and

(3.5);

$$V_{roCCE}(P) = \left[1 + \left(\frac{R_p - R_s}{1 - r_s R_p}\right)\frac{B_{gd}}{B_o}\right]^{-1}. \quad (3.6)$$

Evinger and Muskat, have shown that when both phases are mobile then the k_{rg} *and* k_{ro} can be expressed by the ratio k_{rg}/k_{ro}. If the ratio k_{rg}/k_{ro} is determind then we can easily calculate the values of k_{rg} *and* k_{ro} from the relative permeability curve (figure 3.10) and will be able to evaluate the pseudopressure integral.

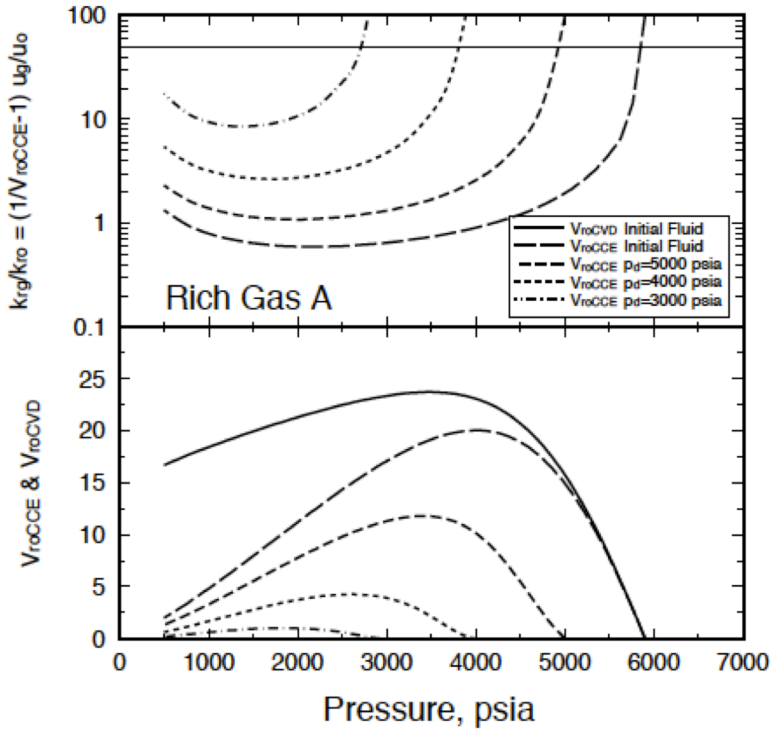

Figure 3.9: Rich gas-condensate plot that explains the variation of k_{rg}/k_{ro} and CCE oil relative volume as a function of pressure during depletion.

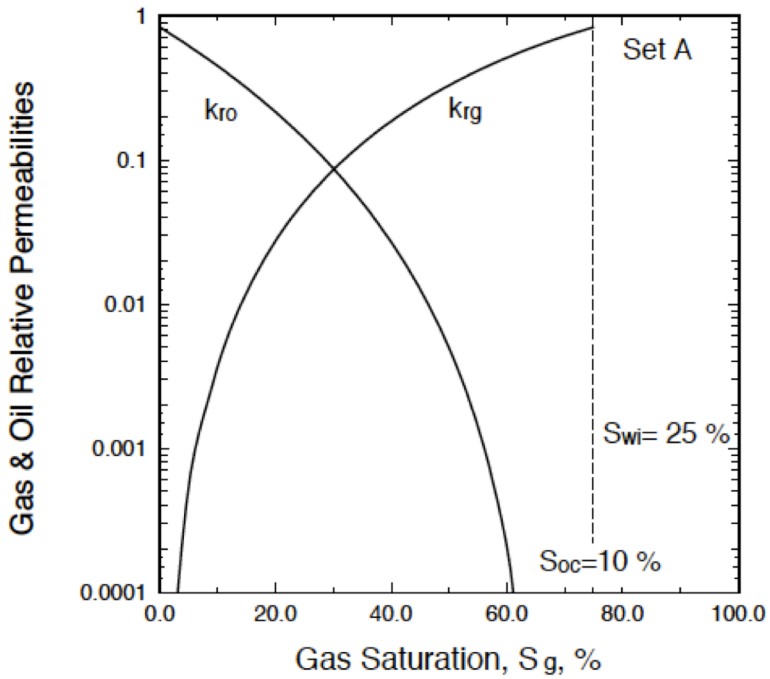

Figure 3.10: The relative permeability curves for oil and gas that are used in the simulation.

Table 6: Reservoir fluid composition (more rich in liquid components) used in the simulations.

Components	Citical Tempreture $Tc, [R]$	Critical Pressure P_c, [psia]	Molecular Weights
CO_2	547.56990	1070.60000	44.00999
N_2	227.26990	493.00000	28.01300
C_1	343.03990	667.80000	16.04300
C_2	549.75990	707.80000	30.07001
C_3	665.67990	616.30000	44.09700
$\mathrm{i}-C_4$	734.64990	529.10010	58.12399
C_4	765.31980	550.70000	58.12399
$i-C_5$	828.77000	490.39990	72.15100
C_5	845.36990	488.60010	72.15100
C_6	913.36990	436.89990	86.17799
C_{7+1}	998.67380	460.38250	96.63251
C_{7+2}	1153.64700	339.88360	142.23400
C_{7+3}	1362.29000	227.69900	228.81020
C_{7+4}	1580.18000	154.48470	367.19530
C_{7+5}	1804.77000	113.15790	587.50000

For this purpose, we have constructed a cylindrical producing single-well with a radial model where the well is located at the center. Using a compositional numerical simulator (Eclipse300), we have been able to construct a rich gas-condensate data for a radial flow model that represents a single well with high drawdown at an infinite-acting period. As we can see from the simulations, output the grid is distributed logarithmically in radial nodes. The size of the innermost node is 0.53ft, while the outer node is 2465.9ft.

The rich gas-condensate reservoir behaves similarly to the lean gas-condensate in such a way that the producing OGR is always below the solution OGR within the infinite acting period at a constant rate. However, the producing OGR seems to stabilize much faster in rich gas-condensate than lean gas-condensate after the immediate drop below the solution OGR.

3.2.1 Producing OGR behaviour

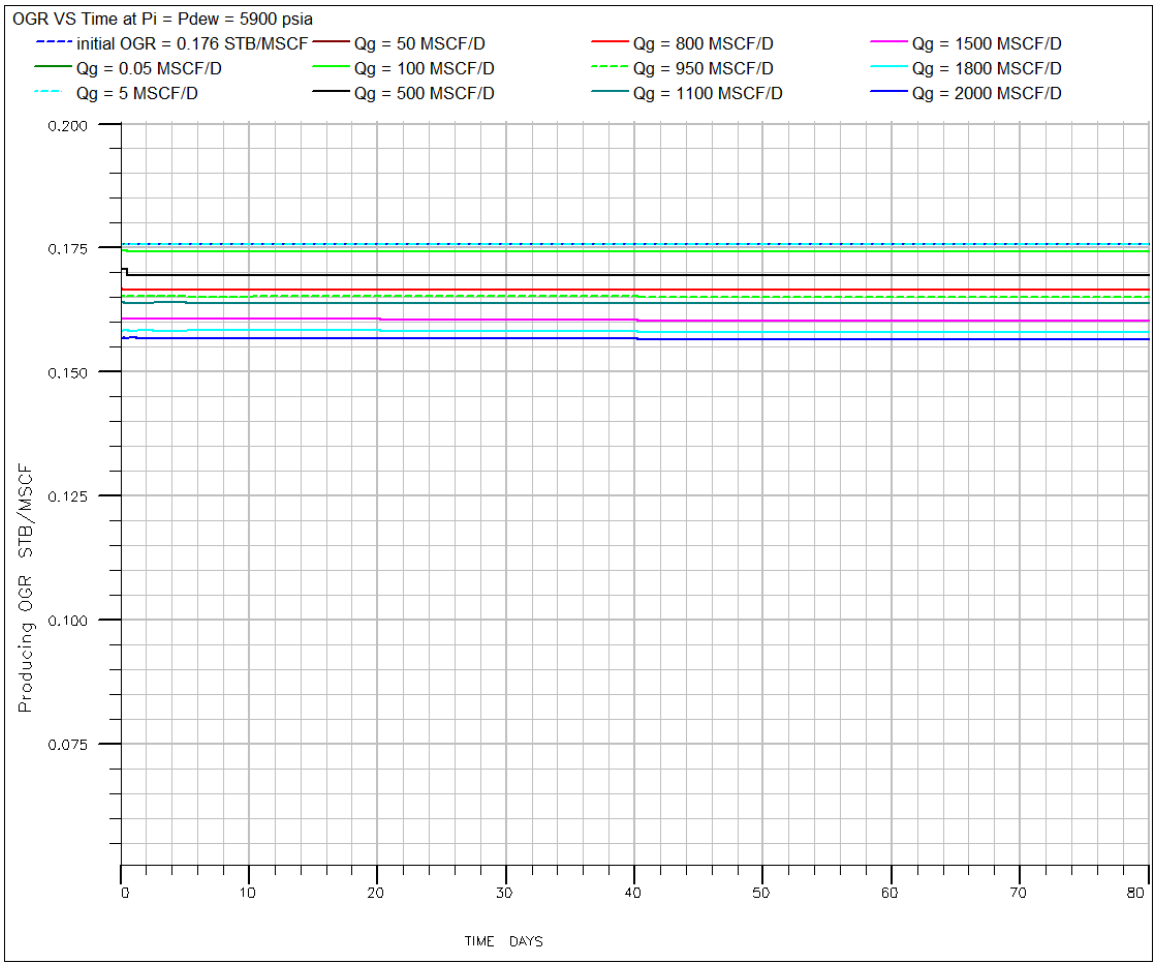

Figure 3.11: Producing OGR behaviour Vs time for rich gas-condensate with corresponding constant surface-gas rate during a drawdown of vertical well.

As we can see from Figure 3.11, the OGR stabilizes from the early simulation period and remains stable through out the entire infinite-acting period at a constant rate. For this particular model the maximum acceptable rate is 2000MSCF/D within the inifite-acting period considering the limiting FBHP is set to be 1500 psia in order to avoid a sudden rate declines.

Figure 3.12 below shows production performance for the rich gas-condensate well producing countinuously with a minimum limiting FBHP of 1500 psia. The producing OGR expiences an immediate drop to about 0.167 STB/MScf and remains constant for the entire infinite-acting peiod of 60 days modeled.

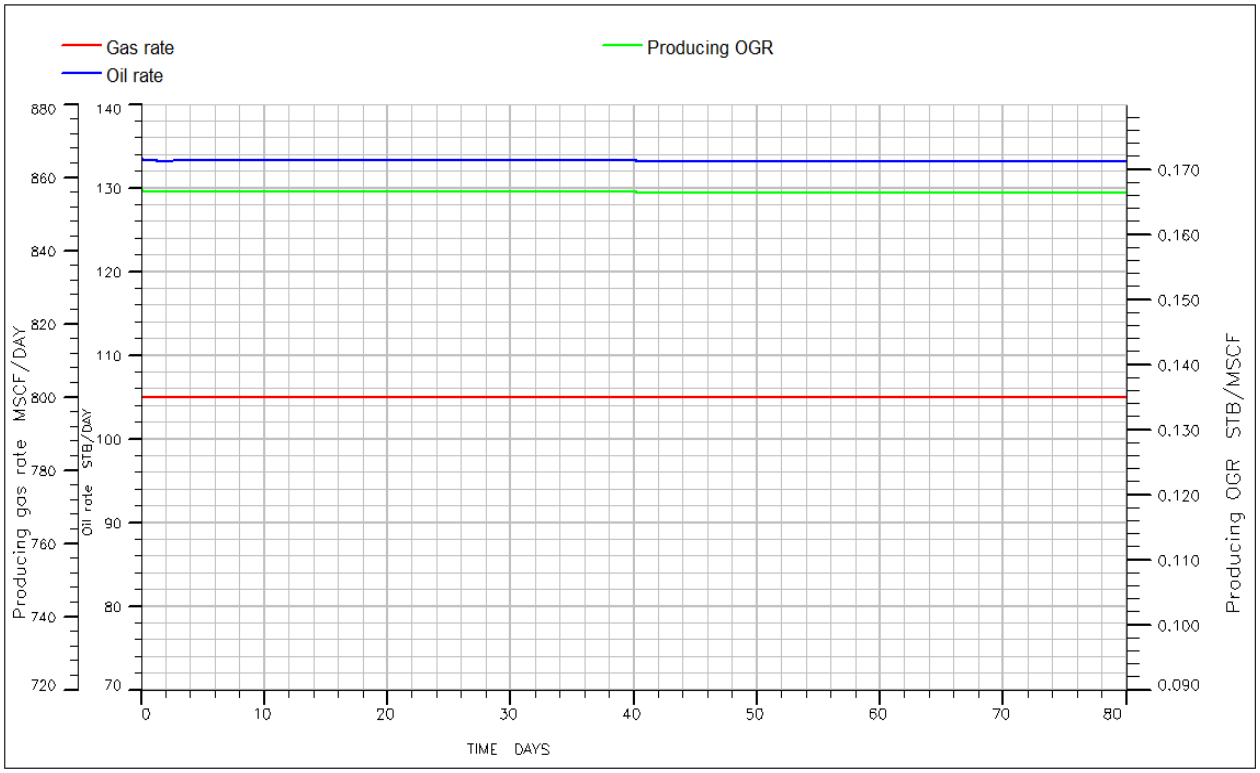

Figure 3.12: Production performance for a well producing against a constant limiting FBHP of 1500psia
($P_{dew} = 5900psia, R_i \approx 5682\ Scf/STB\ , r_i = 0.176\ STB/MScf$).

3.2.2 Well-productivity of rich gas-condensate

The term well productivity is very significant for low permeability rich gas-condensate reservoirs during the development. Generally, gas-condensate reservoir shows some unique behavior in a way that it is characterized by a rapid loss of well productivity. John Evan and Reggie (1998) have explained some of the significant reasons for the reduction of well productivity during the pressure depletion, which is caused due to the buildup of a condensate saturation ring near the wellbore. Numerous amounts of studies indicate that the well productivity is highly affected when the FBHP drops below the dew point pressure. In that case, productivity reduction occurs due to the accumulation of liquid around the well, which literally impairs the gas flow and reduces productivity.

It is always best to determine the well productivity of a single well rich gas-condensate with a numerical simulation of fine-grid, since numerical simulation is

very suitable for better detailed forecasting of gas-condensate reservoir. Parameters such as, PVT properties, rock and water compressibility relative permeability curves (figure 3.10), reservoir data and well geometry (cylindrical in our case) are the most important factors for calculating the well productivity. However, it can be very difficult to predict accurate forecasts considering the advanced and complicated processes that occur in the near-well region, which requires a good understanding.
Note that, it is essential to consider the effect of "condensate blockage" (see section 2.1.2) when calculating the well productivity since the losses can actually be significant. In gas-condensate wells, the gas velocity is very high around the wellbore; hence, most of the drawdown tends to occur close to the wellbore.

Many studies show the several parameters that influence the productivity losses and in this thesis, we have made some investigation on parameters like liquid dropout rate and gas-oil relative permeability. However, several researches imply that the relative permeability as the most sensitive parameter when calculating the well productivity loss. It is necessary to accurately model both the gas relative permeability and condensate saturation in the near wellbore region, because the accumulation of condensate in the near wellbore causes a reduction in gas relative permeability, which in turn reduces the PI. Several laboratory results have been claimed regarding the measurement of the gas relative permeability as a function of interfacial tension (IFT). That is, as a decrease of interfacial tension between the gas and condensate a dramatic increase in gas relative permeability occurs. In such cases, we can directly model the relative permeability of the gas and condensate as a function of IFT.

Robert Mott (2002) showed the well inflow calculation applying the pseudopressure integral formula by introducing the well gas production rate:

$$Q_g = \gamma[m(P_{res}) - m(P_w)]. \tag{3.7}$$

Where,

$$m(P) = \int_{P_{ref}}^{P} \left[\frac{k_{rg}}{\mu_g B_g} + \frac{k_{ro} R_s}{\mu_o B_0}\right] dP. \tag{3.8}$$

Fevang and Whitson have proposed the three flow regions around the well, which can be evaluated by the pseudopressure integral. The detailed discussion regarding the three flow regions around the well has been discussed earlier in chapter 2.

3.3 Black-oil Reservoir

This section describes the numerical model for simulating black-oil reservoir together with their general description of fluid characteristics. We basically classify oil reservoirs according to their fluid type. Based on their increasing order of their molecular weight, they classified as volatile oil, back oil and heavy oil. Among these different oil types, the molecular weight is a significant yardstick that highlights their main differences. The molecular weight of black oil may sometimes reach up to 190 to 210 but it typically is in the ranges of 70 to 150. Volatile oils on the other hand have lower molecular weight and typically ranges from 43 to 70. And as we see from the table below (table 7), the heavy oil tends to have a much higher molecular weight of above 210. The major characteristic difference between black oil and volatile oil is the stock-tank-oil (STO) content of their equilibrium gases. The heavy oil reservoir shows high fluid viscosities and low dissolved-gas contents which make them to yield just a marginal amount of oil. The equilibrium gases that we get from black oil contain a very small amount of STO and due to that reason it is mostly negligible.

Table 7: Characteristics of Petroleum Fluids (Petrowiki)

Characteristic	Oils			Gases	
	Heavy Oils and Tars	Black Oils	Volatile Oils	Gas Condensates	Wet and Dry Gases
Initial fluid molecular weight	210+	70 to 210	40 to 70	23 to 40	<23
Stock-tank-oil color	black	brown to light green	greenish to orange	orange to clear	clear
Stock-tank oil-gravity, °API	5 to 15	15 to 45	42 to 55	45 to 60	45+
C_7-plus fraction, mol%	>50	35 to 50	10 to 30	1 to 6	0 to 1
Initial dissolved GOR, scf/STB	0 to 200	200 to 900	900 to 3,500	3,500 to 30,000	30,000+
Initial FVF, B_{oi}, RB/STB	1.0 to 1.1	1.1 to 1.5	1.5 to 3.0	3.0 to 20.0	20.0+
Typical reservoir temperature, °F	90 to 200	100 to 200	150 to 300	150 to 300	150 to 300
Typical saturation pressure, psia	0 to 500	300 to 5,000	3,000 to 7,500	1,500 to 9,000	—
Volatile-oil/gas ratio, STB/MMscf*	0	0 to 10	10 to 200	50 to 300	0 to 50
Maximum vol% liquid during CCE**	100	100	100	0 to 45	0
OOIP, STB/acre-ft (bulk)	1,130 to 1,240	850 to 1,130	400 to 850	60 to 400	0 to 60
OGIP, Mscf/acre-ft (bulk)	0 to 200	200 to 700	300 to 1,000	500 to 2,000	1,000 to 2,200

*At bubblepoint pressure. **Constant composition expansion of reservoir fluid.

Further details regarding volatile oil and heavy oil will not be covered in this study; our major focus concerning simulation and GOR will be all attached to black oil only. The simulation data that we have constructed is a radial black oil model, which involves 2 components that is, oil with dissolved gas and gas (no dissolved oil). Gas oil ratio (GOR) at the bubble point pressure will be our core of discussion in this section. The term bubble point pressure is defined as the point at which the natural gas dissolved in the reservoir oil begins to come out of solution. It can functionally be expressed as:

$$P_b = f(\gamma_{API}, T, \gamma_g R_s) \tag{3.9}$$

3.3.1 Black-oil reservoir Simulation and GOR effects

In black oil simulation purposes gas oil ratio (GOR) is a commonly used term during exploration and production processes. GOR can simply be defined as the ratio of volumetric flow produced gas to the volumetric flow of oil and gas solution mixtures. The black oil GOR behaves differently from lean and rich gas condensates in a sense that producing GOR shows some unique characteristics. As we have discussed earlier in this section the Producing OGR for both cases of lean gas and rich gas condensates always goes below the initial OGR and at most it can reach up to the same level as the initial OGR.

Generally speaking in black oil reservoirs the producing GOR generally exceeds the initial GOR when the reservoir pressure around the wellbore drops below bubble point. Gas comes out of solution. It is much more mobile and this is reflected as an increase in GOR and such kind of situations almost always happens. L.P. Dake (fundamentals of reservoir engineering) explains that behavior knowing both reservoir and well behaves more or less similarly. For this type of reservoir, in the simplest case we assume there is no oil dissolved in the gas.

It is common to talk about the GOR that refers to the gas dissolved in the oil. Initially the reservoir pressure is greater than saturation pressure ($P_{res} > P_b$) so no gas is liberated in the reservoir. The gas that is produced from a well is the gas dissolved in the oil so at this stage the GOR remains at the initial stage. Later on as the reservoir pressure starts to fall below the saturation pressure ($P_{res} < P_b$), gas begins to liberate. Initially, the volume of gas is small so the saturation of gas in the formation is less than the critical gas saturation ($S_g < S_{g,crt}$) thus
S_g *critical is threshold gas saturation for gas to become mobile*. So the amount of gas dissolved in the oil drops. It means the oil that arrives at the surface has a lower GOR, which indicates that the producing GOR is less that the initial GOR

$(R_p < R_i)$. Finally, as the reservoir pressure drops further, in the reservoir more gas is liberated from the oil. Then saturation of gas becomes larger that critical gas saturation $(S_g > S_{g,crt})$ and the gas begins to flow. At this stage, gas is much more mobile than the oil, so the amount of gas arrives at the surface increases dramatically. This is seen as a sharp rise in the producing GOR.

3.3.2 Determining the Bubble point pressure:

There are several methods at which the bubble point can be determined. In this study we have relayed on our simulated grid results to figure out the bubble point pressure for the black oil model that we have constructed. As the first time step the gas saturation should be zero $(S_{gas} = 0)$ if not, it indicates that the reservoir is below bubble point which will require us to increase the initial pressure and start our simulation all over again. From the last time step checking the $(S_{gas} = 0)$ for all cells showed us that we have not produced enough gas to drop the pressure below the bubble point. It is necessary to increase the number of time steps and reinitiate the simulation until $(S_{gas} = 0)$.

When we have a time step with $(S_{gas} = 0)$ then it is important to check gas saturation at earlier time step and determine the first time step where gas has been detected. This corresponds to the time the pressure reaches the bubble point. At that time step we have examined the pressure and that pressure is taken as the bubble point. To be exact, it will be the grid block pressure for the grid block with the smallest S_{gas}.

In the figure 3.13 below, we have simulated the scenario with the well producing at 100 $SM^3/Days$. The reservoir pressure evidently began to decline continuously and after a certain time gas began to appear in the innermost cells $(S_{gas} > 0)$. From figure 3.13 of the gas saturation map, the green cell indicates a $S_{gas} = 0.00414$ and the next cell i.e the blue cell shows $S_{gas} = 0$. Now looking at the pressure map at the same time step the pressures at the mentioned grid blocks are 157.2 bars and 161.1

bars respectively. This brings us to the conclusion that the bubble point is some where between 157.2 bars and 161.1 bars. A more accurate value can readily be found by plotting $S_{gas}\ Vs$ pressure to get the trend. The bubble point from this trend is then the pressure at $S_{gas} = 0$ which in our case tends to be 160 bars.

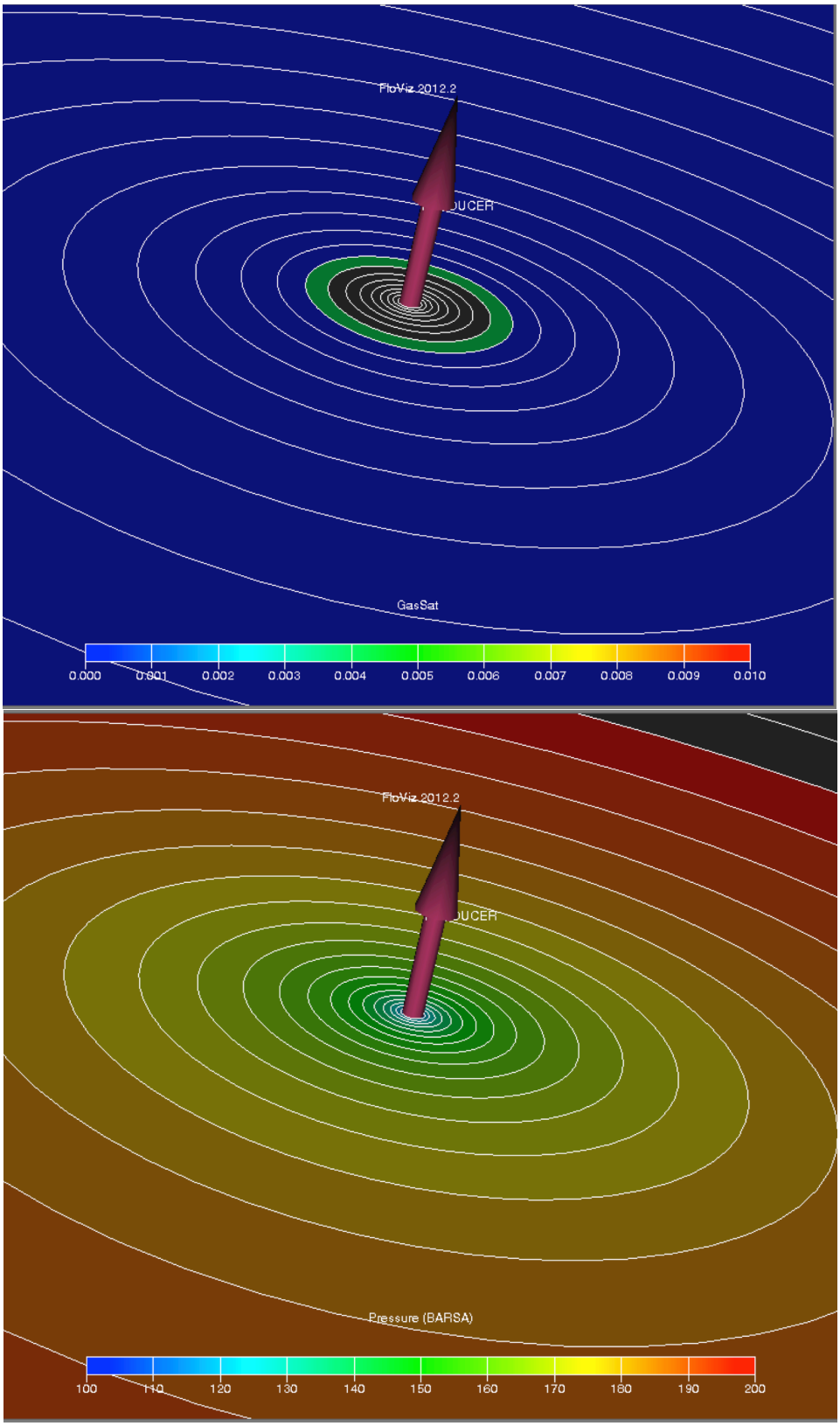

Figure 3.13 Gas saturation and Pressure distribution both of them at the same time step to determine the bubble point pressure.

Having the general GOR concept of black oil reservoir as discussed in section 3.3.1 above we have narrowed our case study within our analyzing conditions. The same way as how we did perform our condensate studies earlier in this section, we have made our investigation for black oil model under the analyzing conditions of infinite-acting period with constant oil flow rate but by varying our choices of the oil rate to a reasonable amount.

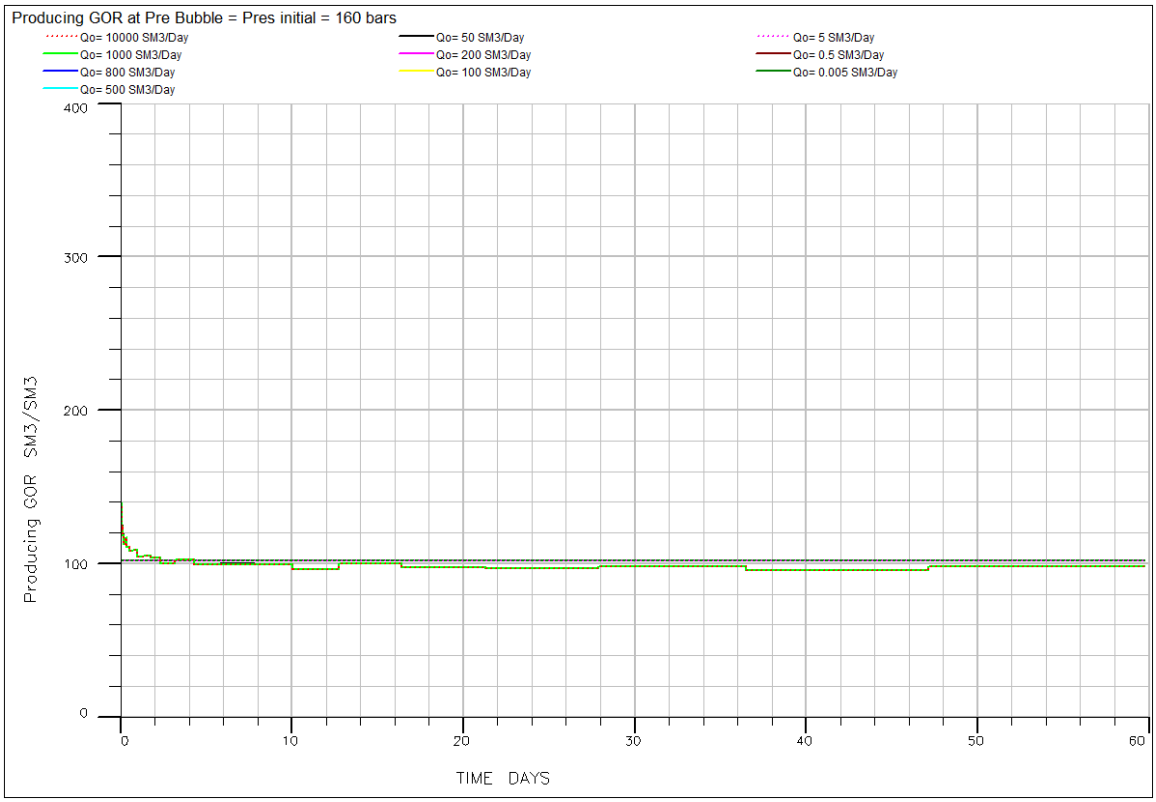

Figure 3.14: Producing GOR Vs time for black oil model with the corresponding constant oil rate but with varius choices of rates.

For an immediate drawdown we have started our simulation with an initial pressure as equal as the saturation pressure.

Chapter 4

The reservoir behaviours are usually described by differential equations that are obtained by combining the law of conservation of mass for each phase in the system together with Darcy's law. This section explains well performance for two-phase flow of hydrocarbons and will briefly explore the concept of Bernoulli equation that has been derived from Riccati equation by Rajagopal Raghavan (1993). To avoid any confusion all the terms and parameters in this chapter have been taken exactly as it from Rajagopal Raghavan (1993).

$$\nabla \cdot G_o + \rho_{os} \frac{\partial}{\partial t}\left(\emptyset \frac{S_o}{B_o}\right) = 0 \tag{4.1}$$

Disregarding the gravity effect, the velocity of phase m is given by Darcy's law as:

$$V_m = -\frac{K_m}{\mu_m B_m} \nabla P. \tag{4.2}$$

By substituting the right hand side of (2) in (1) we have

For oil:
$$\nabla \cdot \left(K \frac{K_{ro}}{\mu_o B_o} \nabla p\right) = \emptyset \frac{\partial}{\partial t}\left(\frac{S_o}{B_o}\right) \tag{4.3}$$

For gas:
$$\nabla \cdot \left[K\left(\frac{K_{rg}}{\mu_g B_g} + R_s \frac{K_{ro}}{\mu_o B_o}\right) \nabla p\right] = \emptyset \frac{\partial}{\partial t}\left(\frac{S_g}{B_g} + R_s \frac{S_o}{B_o}\right). \tag{4.4}$$

If we let $\alpha_o = K_{ro}/\mu_o B_o$, $\beta = S_o/B_o$, $a = K_{rg}/(\mu_g B_g) + R_s \alpha_o$, and $b = S_g/B_g + R_s(S_o/B_o)$ then we can rewrite the above equation of oil and gas respectively as

For oil:
$$\nabla \cdot (K \alpha_o \nabla p) = \emptyset \frac{\partial \beta}{\partial t} \tag{4.5}$$

For gas:
$$\nabla \cdot (K a \nabla p) = \emptyset \frac{\partial b}{\partial t}. \tag{4.6}$$

Rewriting (5) in a gas flow term leads to

$$\nabla \cdot \left[K(\alpha_o + \alpha_g)\nabla p\right] - \nabla \cdot \left(K \alpha_g \nabla p\right) = \emptyset \frac{\partial \beta}{\partial t}. \tag{4.7}$$

Where;

$\alpha_g = K_{rg}/(\mu_g B_g)$

But the α_g can be formulated as shown below in a simplified form knowing the total gas oil ratio (R') and R_s

$$R' = \frac{(K_{rg}/\mu_g B_g)+R_s(K_{ro}/\mu_o B_o)}{(K_{ro}/\mu_o B_o)} \quad \text{that is,} \quad R' = \frac{a}{\alpha_o}$$

thus;

$$\alpha_g = \alpha_o(R' - R_s)$$

$$\nabla \cdot \left[K(\alpha_o + \alpha_g)\nabla p\right] - \nabla \cdot [\mathrm{K}\alpha_o(R' - R_s)\nabla p] = \emptyset \frac{\partial \beta}{\partial t}.$$

From (5) and (6) we have

$$K\alpha_o \nabla p \cdot \nabla R^{'} + R^{'}\emptyset \frac{\partial \beta}{\partial t} = \emptyset \frac{\partial b}{\partial t}. \tag{4.8}$$

Further detailed discussion will be performed based on the above equations of (4.5) and (4.8) respectively by

$$\frac{1}{r}\frac{\partial}{\partial r}\left(r\alpha_o \frac{\partial p}{\partial r}\right) = \frac{\emptyset}{k}\frac{\partial}{\partial t}\left(\frac{S_o}{B_o}\right) \tag{4.9}$$

$$\alpha_o \frac{\partial p}{\partial r}\frac{\partial R'}{\partial r} + R' \frac{\emptyset}{k}\frac{\partial \beta}{\partial t} = \frac{\emptyset}{k}\frac{\partial b}{\partial t}. \tag{4.10}$$

In (4.9) and (4.10) both k and $\emptyset$ are assumed to be constant and assuming the parameters R', β and b to be functions of pressure and saturation, let

$$\xi_p = \emptyset\left(\frac{\partial b}{\partial p} - R'\frac{\partial \beta}{\partial p}\right) \tag{4.11}$$

$$\xi_s = \emptyset\left(\frac{\partial b}{\partial S} - R'\frac{\partial \beta}{\partial S}\right) \tag{4.12}$$

and

$$k\alpha_o \frac{\partial p}{\partial r}\frac{\partial R'}{\partial S} = \frac{q_o(r)}{2\pi hr}\frac{\partial R'}{\partial S} = C'. \tag{4.13}$$

From (4.11) and (4.12), we can rewrite (4.10) as

$$\xi_s \frac{\partial S}{\partial t} + \xi_p \frac{\partial p}{\partial t} = C' \frac{\partial S}{\partial r} + k\alpha_o \left(\frac{\partial p}{\partial r}\right)^2 \frac{\partial R'}{\partial p} \tag{4.14}$$

$$\xi_s \frac{\partial S}{\partial t} = C' \frac{\partial S}{\partial r} + k\alpha_o \left(\frac{\partial p}{\partial r}\right)^2 \frac{\partial R'}{\partial p} - \xi_p \frac{\partial p}{\partial t}$$

$$\frac{\partial S}{\partial t} = \frac{C'}{\xi_s}\frac{\partial S}{\partial r} + \frac{k\alpha_o}{\xi_s}\left(\frac{\partial p}{\partial r}\right)^2 \frac{\partial R'}{\partial p} - \frac{\xi_p}{\xi_s}\frac{\partial p}{\partial t}.$$

Where;

$F = \frac{k\alpha_o}{\xi_s}\left(\frac{\partial p}{\partial r}\right)^2 \frac{\partial R'}{\partial p} - \frac{\xi_p}{\xi_s}\frac{\partial p}{\partial t}$ and $C = -\frac{C'}{\xi_s}$

It then results to

$$\frac{\partial S}{\partial t} + C\frac{\partial S}{\partial r} = F. \tag{4.15}$$

Note: The speed C and the forcing function F are independent of the saturation derivative even though they both are functions of saturation.

By introducing the similarity variable parameter $\eta = r^2/t$ to (15) we then express $dS/d\eta$ in a simplified form

$$\frac{dS}{d\eta} = \frac{\eta + \frac{\emptyset\ \partial R'}{\xi_p\ \partial p}}{\left(\eta + \frac{\emptyset\ \partial R'}{\xi_s\ \partial S}\right)}\left(\frac{\xi_p}{-\xi_s}\right)\frac{dp}{d\eta}. \tag{4.16}$$

Where;

$\emptyset(\eta) = \frac{q_o}{\pi h} = 4k\alpha_o \eta \frac{dp}{d\eta}.$

For large values of η: $\frac{dS}{d\eta} \approx \frac{\xi_p}{-\xi_s}\frac{dp}{d\eta}$ (4.17)

Assuming all second degree terms are negligible the previously introduced equation of (4.3) and (4.4) will be written respectively

$$\frac{\lambda_o}{B_o}\nabla^2 p = \frac{\emptyset}{k}\frac{d\beta}{dt}$$

and (4.18)

$$\left(\frac{\lambda_g}{B_g} + \frac{\lambda_o R_s}{B_o}\right)\nabla^2 p = \frac{\emptyset}{k}\frac{db}{dt}.$$

After combining both these equation in (4.18) we may end up having

$$\left(\frac{\lambda_g}{\lambda_o}\frac{B_o}{B_g} + R_s\right)\frac{d\beta}{dp} = \frac{db}{dp} \tag{4.19}$$

or

$$\frac{dS_o}{dp} = \frac{S_o}{B_o}\frac{dB_o}{dp} + \frac{\lambda_o}{\lambda_t}C_t. \tag{4.20}$$

Substituting for ξ_s/ξ_s terms in (4.17), is $S = S_o$then (4.17) yields (4.20). From (4.16) we can show that at long times that is $(\eta \to 0)$, we have $\frac{\partial R'}{\partial p} = 0$ which indicates that the R'must tend to a constant at the wellbore. Thus,

$$R'(r_w) = R = R_s + \frac{k_g}{k_o}\frac{\mu_o}{\mu_g}\frac{B_o}{B_g} \approx constant.$$

We can now express (4.10) in terms of the Boltzmann variable (1984)

$$\eta\emptyset\left(\frac{db}{d\eta} - R'\frac{d\beta}{d\eta}\right) + \emptyset\frac{dR'}{d\eta} = 0 \tag{4.21}$$

(4.9) can be expressed in terms of Boltzmann variable together with (4.21), that is

$$\frac{d\emptyset}{d\eta} = -\frac{\emptyset^2}{4\emptyset\frac{k\alpha_o}{\emptyset}R'\eta}\frac{dR'}{dp} - \frac{\emptyset}{4\frac{k\alpha_o}{\emptyset}\frac{R'}{\frac{db}{dp}}} \tag{4.22}$$

$$\frac{d\emptyset}{d\eta} = -\frac{\emptyset^2}{4k\alpha_o R'\eta}\frac{dR'}{dp} - \frac{\emptyset}{4k\alpha_o}\frac{\frac{db}{dp}}{R'}.$$

We can write (4.22) in a simplified form of

$$\frac{d\emptyset}{d\eta} = \frac{\Lambda\emptyset^2}{\eta} - \frac{\emptyset}{4D} \tag{4.23}$$

For,

$$D = \frac{D^*R'}{\frac{db}{dp}} \qquad and \qquad \Lambda = -\frac{\emptyset^2}{4kD^*R'}\frac{dR'}{dp}.$$

Where;

$$D^* = \frac{k\alpha_o}{\emptyset}$$

As it has been mentioned earlier in this section $b, \beta \; and \; R'$ are functions of saturation, therefore the expression of $dS/dp \;\; i.e \; dR'/dp \;\; and \;\; db/dp$, which are in Λ and D respectively, will be obtained from (4.16). The coefficients in (4.23) needed to be considered constant in order to obtain the solution for (4.23). The nonlinear differential equation shown in (4.23) is one of the most used equations in the oil-gas system and is known as *Riccati equations*.

4.1 General form of Riccati equation

Compared to the linear differential equation the nonlinear differential equations may be much more complicated to solve them but in most cases we will still be able to solve them regardless of how complicated they are. The *Riccati equation* is one of the most important *nonlinear differential equations of first order*. It is expressed in so many different ways and it refers to any first-order differential equation that is quadratic in the unknown function as shown below.

$$\frac{dy}{dx} = A(x)y^2 + B(x)y + C(x). \tag{4.24}$$

It is known that all types of Riccati equations can always be simplified to a second order linear ODE

By substitution $y = -\frac{v'}{v*A}$

$$v'' - \left[B(x) + \frac{A'(x)}{A(x)}\right]v' + C(x)A(x) = 0$$

Where $A(x) \neq 0 \; and \; C(x) \neq 0$ but if $C(x) = 0$ then (4.24) reduces to a *Bernoulli equation*, while if $A(x) = 0$ the equation becomes a first order linear ordinary differential equation (ODE). Assuming y, A, B and C are continuous functions of x from

$$y' = Ay^2 + By + C.$$

Note: If a particular solution g of a Riccati equation is given, then the transformation:

$$y = g + \frac{1}{u} \tag{4.25}$$

reduces it to a linear equation in u.

Considering g is a particular solution of (4.24), so just substitute g into (4.24), yielding:

$$g' = Ag^2 + Bg + C. \tag{4.26}$$

But having the transformation (4.25), so lets us it, we have $\left(y = g + \frac{1}{u}\right), so$

$$y' = g' - \frac{1}{u^2}u' = (Ag^2 + Bg + C) - \frac{1}{u^2}u' \tag{4.27}$$

From (4.24) we have

$$y' = Ay^2 + By + C = A\left(g + \frac{1}{u}\right)^2 + B\left(g + \frac{1}{u}\right) + C. \tag{4.28}$$

Equating (4.27) and (4.28) and collecting like terms leads to:

$$-\frac{1}{u^2}u' = A\frac{1}{u} + 2gA\frac{1}{u} + B\frac{1}{u} \tag{4.29}$$

Simplifying (4.29) yields:

$$u' + (B + 2gA)u = -A. \tag{4.30}$$

Using the given assumptions and parameters from the above equations, Rajagopal Raghavan (1993) then expressed the final equations as;

$$S_i - S(\eta) = \left(\frac{\xi_p}{-\xi_s}\right)\frac{C_1}{4k\alpha_0}\left[-Ei\left(-\frac{\eta}{4D}\right)\right] + \left(-\frac{1}{\xi_s}\right)\frac{C_1^2}{4k\alpha_0}\frac{1}{\eta}\frac{\partial R'}{\partial p}E_2\left(\frac{\eta}{2D}\right). \tag{4.31}$$

Where;

$q_0(\eta^*) = \pi h C_1$ and from Abramovitz and Stegyn (1972) $E_2\eta = e^{-\eta} + \eta Ei(-\eta)$.

Most of the parameters in (4.31) involve a partial differential equation (PDE), which makes (4.31) very complicated to deal as it is; therefore we have suggest to divide

into smaller equations as much as possible in such a way that could be simply defined in order to solve it either numerically or analytically.

As we can see the right hand side (RHS) of equation 4.31 involves several parameters that are functions of pressure and saturation, which have been defined earlier in this section. We can take a good representative sample when $S_i - S(\eta) = 0$ or somewhat closer to zero which indicates a stabilized producing GOR lever closer to the initial GOR. Increasing the permeability (K) would definitely tend to create flat pressure profile and lowers the RHS of equation 12.113, however K is a constant parameter that cannot be controlled. Knowing η is a function of the well radius (r_w) then for higher r_w at any given time the saturation $S(\eta)$ will be closer to the value of S_i which will make their difference to be somewhere closer to zero.

Referring back to chapter-3, we have concluded that lower surface flow rate as the best testing parameter for taking a better representative sample. Lower flow rate (q_o), which, is a function of C_1 in 4.31 makes higher drawdown and slower changes with small pressure drop(ΔP). Increasing compressibility itself would tend to make processes to happen slower. Because, as 4.31 below shows an increase in C_t will cause lower pressure drop (ΔP).

$$C_t = \frac{\Delta V}{V\,\Delta P}$$

4.2 Recommended Solving methods

The above-discussed equation 4.31 can possibly be solved both numerically and analytically by different methods and procedures. Due to shortage of time we couldn't finish solving this equation however, we have initiated some possible solving methods and we might reach to the final solution later in a very near future.
From equation 4.31;

$$S_i - S(\eta) = \left(\frac{\xi_p}{-\xi_s}\right)\frac{C_1}{4k\alpha_0}\left[-Ei\left(-\frac{\eta}{4D}\right)\right] + \left(-\frac{1}{\xi_s}\right)\frac{C_1^2}{4k\alpha_0}\frac{1}{\eta}\frac{\partial R'}{\partial p}E_2\left(\frac{\eta}{2D}\right)$$

In order to take the correct sample it is necessary for the saturation pressure to be zero or somewhere closer to zero, $i.e$

$$S_i - S(\eta) = 0$$

$$\left(\frac{1}{-\xi_s}\right)\frac{C_1}{4k\alpha_0}\left[\xi_p\left[-Ei\left(-\frac{\eta}{4D}\right)\right] + \frac{C_1}{\eta}\frac{\partial R'}{\partial p}E_2\left(\frac{\eta}{2D}\right)\right] = 0$$

$$\xi_p\left[-Ei\left(-\frac{\eta}{4D}\right)\right] + \frac{C_1}{\eta}\frac{\partial R'}{\partial p}E_2\left(\frac{\eta}{2D}\right) = 0 \tag{4.32}$$

$$\text{Knowing} \quad b = S_g/B_g + R_s(S_o/B_o) \quad and \quad \xi_p = \emptyset\left(\frac{\partial b}{\partial p} - R'\frac{\partial \beta}{\partial p}\right) \tag{4.33}$$

We have then differentiated b with respect to the pressure by applying the chain rule,

$$\frac{u}{v} = \frac{v\,du/dx - u\,dv/dx}{v^2}$$

$$\frac{\partial b}{\partial p} = \frac{-\left[B_g(S_g)_P - S_g(B_g)_P\right]}{B_g^2} + \left[R_S\frac{S_o}{B_o}\right]_P. \tag{4.34}$$

But $R_s = \frac{Volume\ of\ gas}{Volume\ of\ oil}$

$$R_s = \frac{S_g V_p}{S_o V_p} = \frac{S_g}{S_o}$$

$S_g + S_o + S_{wr} = 1$ Which on the other hand gives, $S_g = \frac{(1-S_{wr})}{(1+R_S)}$ and $S_o = \frac{(1-S_{wr})}{\left(\frac{1}{R_S}+1\right)}$.

Therefore,

$$\frac{\partial S_g}{\partial p} = \frac{-(1-S_{wr})}{(1+R_s)^2}\,(R_s)_p$$

and

$$\frac{\partial S_o}{\partial p} = \frac{(1 - S_{wr})}{\left(1 + \frac{1}{R_s}\right)^2} \frac{1}{{R_s}^2} (R_s)_p$$

$$\frac{\partial S_o}{\partial p} = \frac{(1 - S_{wr})}{(1 + R_s)^2} (R_s)_p$$

Now equation 3.34 becomes,

$$\frac{\partial b}{\partial p} = \frac{-B_g (S_g)_P + S_g (B_g)_P}{B_g^2} + \left[\frac{S_g}{B_o}\right]_P$$

$$\frac{\partial b}{\partial p} = \frac{-B_g (S_g)_P + S_g (B_g)_P}{B_g^2} + \left[\frac{S_g}{B_o}\right]_P$$

$$\frac{\partial b}{\partial p} = \frac{-B_g (S_g)_P + S_g (B_g)_P}{B_g^2} + \frac{B_o (S_g)_P - S_g (B_o)_P}{B_o^2}$$

$$\frac{\partial b}{\partial p} = (S_g)_P \left[\frac{1}{B_o} - \frac{1}{B_g}\right] + S_g \left[\frac{(B_g)_P}{B_g^2} - \frac{(B_o)_P}{B_o^2}\right]$$

$$\frac{\partial b}{\partial p} = \frac{-(1-S_{wr})}{(1+R_s)^2} (R_s)_p \left[\frac{1}{B_o} - \frac{1}{B_g}\right] + S_g \left[\frac{(B_g)_P}{B_g^2} - \frac{(B_o)_P}{B_o^2}\right]. \quad (4.35)$$

$$\beta = \frac{S_o}{B_o}$$

$$\frac{\partial \beta}{\partial p} = \frac{\partial}{\partial p}\left(\frac{S_o}{B_o}\right) = \frac{B_o(S_o)_P - S_o(B_o)_P}{B_o^2}$$

$$\frac{\partial \beta}{\partial p} = \frac{1}{B_o^2}\left[B_o \frac{(1 - S_{wr})}{(1 + R_s)^2}\,(R_s)_p - S_o(B_o)_P\right] \tag{4.36}$$

From (4.35) and (4.36), equation (4.33) then becomes,

$$\xi_p = \emptyset\left(\frac{(1-S_{wr})}{(1+R_s)^2}\,(R_s)_p\left[\frac{1}{B_g} - \frac{1}{B_o}\right] + S_g\left[\frac{(B_g)_P}{B_g^2} - \frac{(B_o)_P}{B_o^2}\right] - R'\frac{1}{B_o^2}\left[B_o\frac{(1-S_{wr})}{(1+R_s)^2}\,(R_s)_p - S_o(B_o)_P\right]\right) \tag{4.37}$$

Knowing $\eta = \frac{r^2}{t}$ and $D = \frac{D^* R'}{\frac{db}{dp}} = \frac{\frac{k\alpha_o}{\emptyset}R'}{\frac{db}{dp}}$

$$\frac{\eta}{4D} = \frac{r^2 * \emptyset * \frac{db}{dp}}{t * 4 * k\alpha_o R'}$$

$$E_i\left(\frac{\eta}{4D}\right) = E_i\left(\frac{r^2 * \emptyset * \frac{db}{dp}}{t * 4 * k\alpha_o R'}\right) \tag{4.38}$$

and

$$E_2\left(\frac{\eta}{2D}\right) = E_2\left(\frac{r^2 * \emptyset * \frac{db}{dp}}{t * 2 * k\alpha_o R'}\right)$$

but

$$E_2(\eta) = e^{-\eta} + \eta E_i(-\eta)$$

Thus,

$$E_2\left(\frac{\eta}{2D}\right) = e^{-\frac{\eta}{2D}} + \frac{\eta}{2D} E_i\left(-\frac{\eta}{2D}\right)$$

where

$$\frac{\eta}{2D} = \frac{r^2 * \emptyset * \frac{db}{dp}}{t * 2 * k\alpha_o R'}$$

From the definition given in the previous section $R' = \frac{a}{\alpha_o}$ where $\alpha_o = K_{ro}/\mu_o B_o \ and \ a = K_{rg}/\left(\mu_g B_g\right) + R_s \alpha_o$

$$R' = \frac{K_{rg}/\left(\mu_g B_g\right) + R_s \alpha_o}{\alpha_o} = \frac{K_{rg}}{\mu_g B_g \alpha_o} + R_s$$

$$R' = \frac{K_{rg}\mu_o B_o}{K_{ro}\mu_g B_g} + R_s$$

$$\frac{\partial R'}{\partial p} = \frac{\mu_o}{\mu_g}\frac{\partial}{\partial p}\left[\frac{K_{rg}B_o}{K_{ro}B_g}\right](R_s)_p \qquad (4.39)$$

Using the above equations we can then evaluate all the parameters in the equations as a function of pressure, which then can be used to find out pressure value that satisfies equation (4.32).

Chapter 5

Conclusions and Recommendations

5.1 Overview

This thesis has looked and provided the behaviors of the producing OGR with respect to the solution OGR by differing specific parameters like surface flow rate, permeability, grid block size and so on. Throughout this entire study, we have made our investigations by setting the analyzing conditions of simulation $i.e$ infinite-acting period, constant surface flow rate and high drawdowns.

The infinite-acting period has ben discussed in details in section 2.4.1. Bøe et al. (1989) have performed some studies for a vertical well in a radial and 1D gas reservoir regarding constant characteristics of GOR analytically within the infinite-acting period. Our numerical simulation studies were for 2D radial well in cylindrical reservoirs of both black oil and compositional. In both cases our simulation results showed a stabilized producing OGR for a longer period of about 60 days (infinite-acting period), which agrees with Bøe et al analytical solution.

5.2 Summary

→ ***Sensitivity of producing OGR with saturation pressure***: we kept the initial pressure as equal to the saturation pressure during our simulation process in order to get an immediate drawdown. According our simulation results for a lean gas-condensate the producing OGR stabilizes in a very short period once it drops away from the initial OGR where as for the rich gas-condensate on the other hand the producing OGR stabilizes from the very beginning. For both gas-Condensate cases the producing OGR never reached anywhere above the initial OGR no matter what surface flow rate or any condition has been applied but it could be possible to get somewhere closer to the initial OGR at very low flow rates. Black oil reservoirs on the other hand, their producing GOR reaches to the level above the initial GOR by showing a sharp rise for a very short period of time before it actually drops down again.

→ ***Sensitivity of producing OGR with the surface flow rate***: the producing OGR is highly influenced by the surface flow rate. Higher surface flow rates tend to lower the producing OGR values away from the initial OGR level. Applying a minimum possible and reasonable flow rate is the best option to get a producing OGR more or less equal to or closer to the initial OGR level for taking a good sample eventually.

→ ***Sensitivity of producing OGR to the relative permeability:*** the relative permeability for gas-oil that are set for different values seems to show variation in the producing OGR difference depending on how high the surface flow rate is. For example, when we take a look on two different cases $i.e\ k_{rg} = k_{ro} = 1\ and\ k_{rg} = k_{ro} = 2$ with two different surface flow rates of $Q_g = 100\, Sm^3/d\ and\ Q_g = 200\, Sm^3/d$. When we apply a $Q_g = 100\, Sm^3/d$ the difference in the Producing OGR between the two different gas-oil permeability cases is almost negligible but with a rate of $Q_g = 200\, Sm^3/d$ the difference between their producing OGR is significant enough to consider. See the figures below:

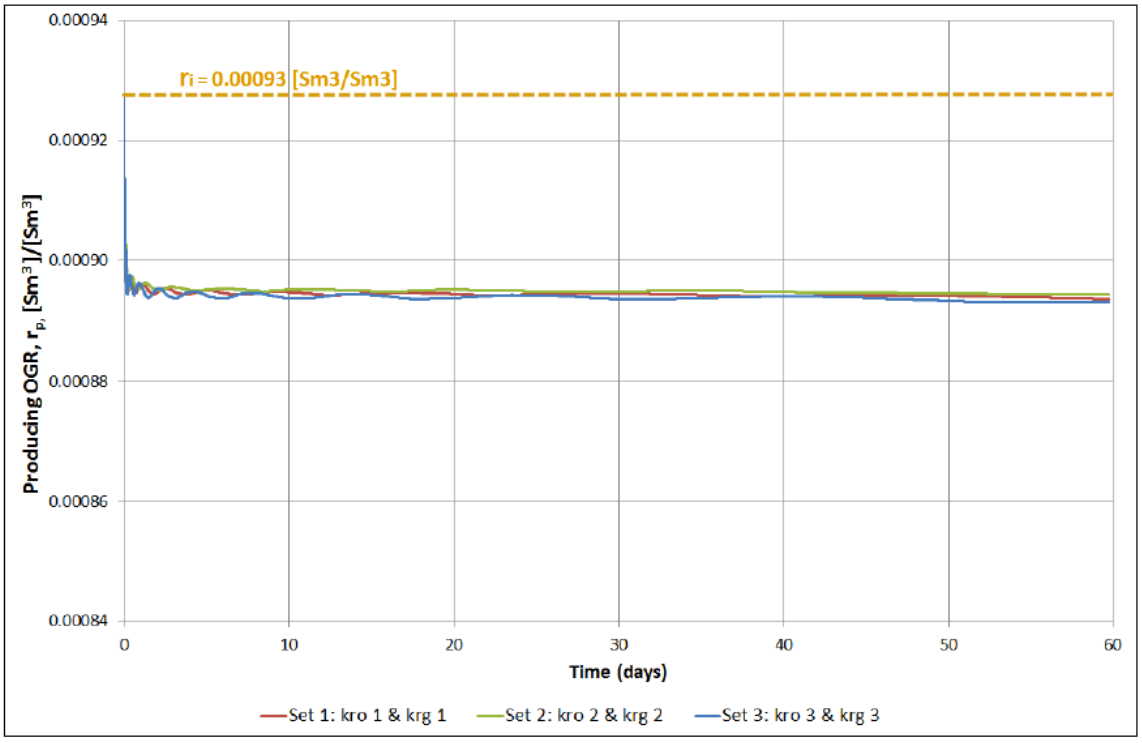

Figure 5.1: The producing OGR effects of a 2D radial compositional model with different relative permeability and a surface flow rate of $Q_g = 100\, Sm^3/d$.

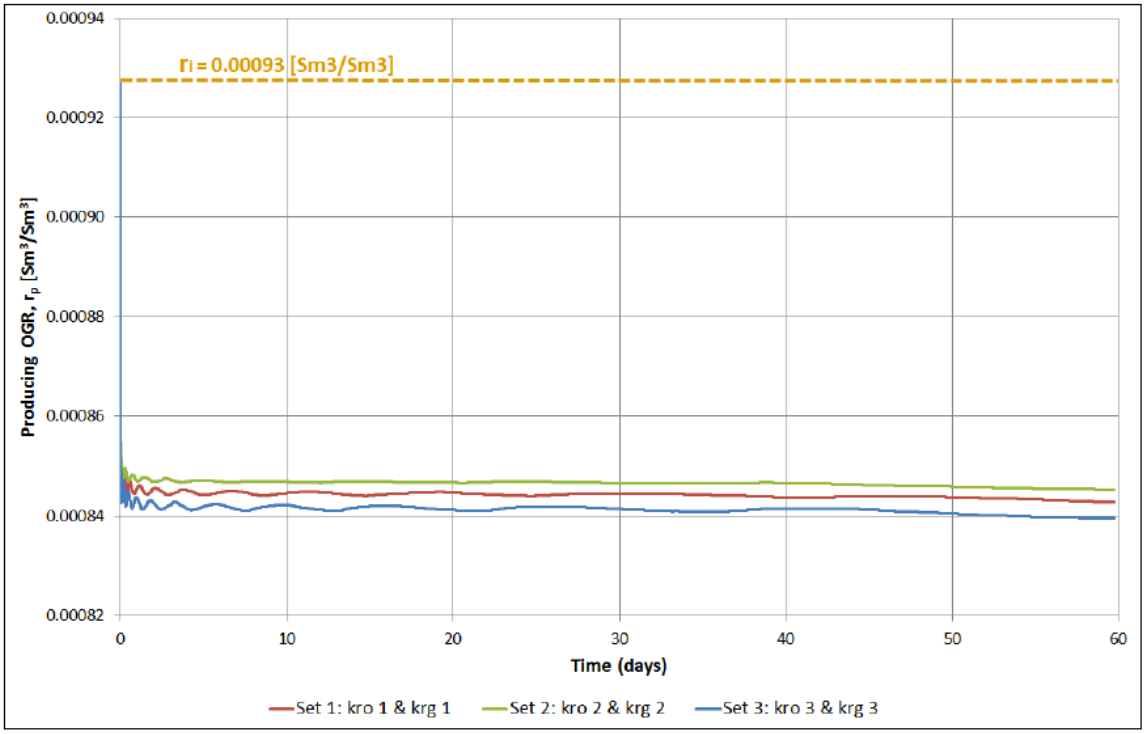

Figure 5.2: The producing OGR effects of a 2D radial compositional model with different relative permeability and a surface flow rate of $Q_g = 200\, Sm^3/d$.

→ ***Stability of OGR within infinite-acting period and FBHP:*** we have narrow our studies by specifying some analyzing conditions and targeting the limiting FBHP to a certain value. The entire data constructing and simulation in this study has been performed under the condition that the boundary not reached and the flow rate could only increase to a certain limit to avoid any fast declination in rate when it goes out of the limiting FBHP specified for each reservoir cases. And we have been making some adjustments to avoid the danger of not converging by increasing the flow rate optimally with respect to the FBHP and increasing the number of grid blocks and decreasing the number of time steps with some factors.

5.3 Conclusion

We can sum up our results by explaining the conditions at which we should test out condensate and oil reservoirs in a way that can give us a correct rate where appropriate and correct samples can be taken. In addition we have also seen we have also explain some of the main reason of a constant OGR at infinite-acting

period and describes fluid sampling conditions and procedures. Our research was for low permeable reservoirs of 2D compositional and back oil at infinite-acting period of radial reservoirs. The flow rate is found as the most affecting and deciding factor for the producing OGR and low flow rate is the best option to get the correct sample. The producing OGR never gets to any level above the initial OGR for condensate reservoirs but at most it can reach to the same level as the initial OGR. However, for black oil reservoirs the producing GOR shows a sharp increase above the initial GOR level for a very short period and drops down again. In both compositional and black oil models the producing OGR and GOR respectively remains constant for the entire infinite-acting period. In low permeability reservoir it may be difficult to get an accurate recombined gas and oil PVT samples when the producing OGR level deviates away from the initial OGR level.

5.4 Recommendation

As we have mentioned in the conclusion above, we strongly recommend taking a sample at low rate since the producing OGR varies depending on the amount of rate we apply. We also suggest to start simulating at an initial pressure equal to the saturation pressure *i. e* dew point pressure and bubble point pressure respectively for gas-condensate and black oil reservoirs when testing the reservoir to get a correct recombined oil-gas PVT sample.

- Further studies can be performed by involving some parameters like skin factor, non-Darcy effects and capillary forces.
- It would be of some interest if more advanced and detailed researches can be made for equation 4.31 both analytically and numerically to the point where the difference between the saturation can be zero or closer to zero.

References

Afidick, D., Kaczorowski, N.J., and Bette, S. 1994. Production Performance of a Retrograde Gas Reservoir: A Case Study of the Arun Field. Presented at the SPE Asia Pacific Oil and Gas Conference, Melbourne, Australia, 7-10 November 1994. SPE-28749-MS.

Al Hussainy R. and Ramey H., *Application of Real Gas Flow Theory to Well Testing and Deliverability Forecasting,* Journal of Petroleum Technology, Volume 18, Number 5, pp. 637-642, May, 1966.

Al Hussainy R., Ramey H. and Crawford P., *The Flow of Real Gases Through Porous Media,* Journal of Petroleum Technology, Volume 18, Number 5, pp. 624-636, May, 1966.

Amin Mirhaseli Igder#1, Abdolnabi Hashemi*2 Department of Petroleum Engineering at petroleum University of Technology (2012) “Pressure Transient Alalysis of a Gas-Condensate Well by Analytical and Numerical Models.

Carlslaw, H.S. and Jaeger, J.C.: “Conduction of Heat in Solids” Oxford University Press, second edition (1959).

Chunmei Shi “ Flow Behavior of Gas-Condensate Wells” A DISSERTATION SUBMITTED TO THE DEPARTMENT OF ENERGY RESOURCES ENGINEERING AND THE COMMITTEE ON GRADUATE STUDIES OF STANFORD UNIVERSITY IN PARTIAL FULFILLMENT OF THE REQUIREMENTS FOR THE DEGREE OF DOCTOR OF PHILOSOPHY in March 2009.

Coats, K. H.: “Simulations of Gas Condensate Reservoir Performance,” JPT (Oct. 1985) 1870.

Curtis Whitson, SPE 155499 “PVT in Liquid-Rich Shale Reservoirs” 2012.

Curtis H. Whitson, Øivind Fevang and Aud Aævareid "Gas Condensate Relative Permeability for well Calculations" Norwegian University of Science and Technology, NTNU, Norway. Received 5 October 2001; in final form: 28 October 2002.

Dake, L.P.: "*Fundamentals of Reservoir Engineering"*, Elsevier Publishing, Oxford (1978).

Danesh, A.: *PVT and Phase Behaviour of Petroleum Reservoir Fluids*, Elsevier Publishing, Netherlands (1998).

Evinger, H.H. and Muskat, M: "Calculation of Theoretical Productivity Factor, " Trans., AIME (1942) 146, 126-139

Fan et al., Understanding gas condensate reservoir 2005, (http://edces.netne.net/files/02_understanding_gas_condensate.pdf)

Fevang, Ø.: 1995, "*Gas Condensate Flow Behavior and Sampling"*, PhD thesis, Norges Tekniske Høgskole.

Fevang, Ø., and Whitson C.H.: "Modeling Gas-Condensate Well Deliverability," paper SPE 30714 first presented at the 1995 SPE Annual Technical Conference and Exhibition, Dallas, Oct. 22-25. Revised manuscript recieved 28 May 1996.

Henderson G. D., Danesh A., Tehrani D. H. and Peden J. M., "*The Effect of Velocity and Interfacial Tension on the Relative Permeability of Gas Condensate Fluids in the Wellbore Region",* Paper Presented at the 8th IOR Symposium, Vienna, Austria, 15–17 May, 1995.

H.R. Zhang, *SPE Member, and R.J. Wheaton, BG International, Reading, Berkshire RG6 1PT, England, UK. "Condensate Banking Dynamics in Gas Condensate Fields: Changes in Produced Condensate to Gas Ratios" (2000)

Johannes Bon and Hemanta Sarma (Australian School of Petroleum, University of Adelaide) Teof Rodrigues and Jan Bon, Reservoir-Fluid Sampling Revisited A practical Perspective (2006).

McCain Jr., W.D., and Alexander, R.A.: “Sampling Gas-Condensate Wells,” paper SPE 19729 presented at the 1989 SPE Annual Technical Conference and Exhibition, San Antonio, Oct. 8-11.

Nagarajan, N.R., Honarpour, M.M., and Sampath, K.: “Reservoir Fluid Sampling and Characterization-Key to Efficient Reservoir Management,” paper SPE 101517 presented at the 2006 Abu Dhabi International Petroleum Exhibition and Conference, Abu Dhabi, U.A.E., Nov. 5-8.
Rajagopal Raghavan “Well Test Analysis” (1993).

Robert Mott (2002) “Engineering calculations of gas condensate well productivity” SPE 77551 (2002).

Shaosong Xu and W. John Lee, Texas A&M U. SPE 55992 “Gas Condensate Well Test Analysis Using a Single-Phase Analogy” 1999.

SPE monograph, v.20

Tarek Ahmed, SPE Montana Tech; John Evans, SPE Montana Tech; Reggie Kwan, Montana Tech and Tom Vivian, Montana Power Company Wellbore Liquid Blockage in Gas-Condensate Reservoirs (1998).

"Theory and Practice of the Testing of Gas Wells, Third Edition", Energy Resources Conservation Board (ERCB), pp. 3-34 to 3-36, 1975

W.D.McCaln Jr., and R.A Alexander,SPE Cawley, Gillespie & Assoccs. Inc. Sampling Gas-Condensate Wells (1992).

Nomenclature

A Reservoir drainage area, $m^2\ or\ ft^2$

B_{gd} Dry gas formation volume factor (FVF), $RB/Scf\ or\ Sm^3/Sm^3$

B_g Gas formation volume factor, $RB/Scf\ or\ Sm^3/Sm^3$

B_o Oil formation volume factor, $RB/Scf\ or\ Sm^3/Sm^3$

c_t Total compressibility, $bar\ or\ psia^{-1}$

E_g Empirical parameter for gas phase

E_o Empirical parameter for oil phase

h Reservoir thickness, $m\ or\ ft$

k Absolute permeability, mD

k_r Relative permeability,

k_{rg} Gas relative permeability

k_{ro} Oil relative permeability

kh Flow capacity, $md.ft$

L_g Empirical parameter for gas

L_o Empirical parameter for gas

$m(p)$ Real gas pseudo-pressure, $psia^2/cP$

M Molecular weight

P_b Bubble point pressure, $psia\ or\ bar$

P_c Critical pressure, bar

P_d Dew point pressure, $bar\ or\ psia$

$P_D(X_D, t_D)$ Dimensionless pressure
$\overline{P_D}$ Dimensionless average pressure

P_{res} Initial reservoir pressure, $bar\ or\ psia$

P_{sc} pressure at standard condition, $1.01325\ bar\ or\ 14.7\ psia$

P_{wf} Flowing bottomhole pressure, $bar\ or\ psia$

$P_{wf,min}$ minimum or target BHFP, $bar\ or\ psia$

P^* Pressure at the boundary between Region 1 and Region 2, $psia\ or\ Pa$

Q_g Surface gas rate, $MScf/d\ or\ Sm^3/d$

r_e External drainage radius, $m\ or\ ft$

r_i Initial oil-gas ratio, Sm^3/Sm^3

r_{inv} Radius of investigation, $m\ or\ ft$

r_p Producing Oil-Gas ratio, Sm^3/Sm^3

r_{pD} Dimensionless producing OGR

r_s Oil dissolved in the gas phase i.e solution OGR, Sm^3/Sm^3

r_w Well radius, $m\ or\ ft$

R' Total gas-oil ratio

R_i Initial Gas-Oil Ratio, Sm^3/Sm^3

R_p Producing Gas-Oil ratio, Sm^3/Sm^3

R_s Gas dissolved in the oil phase i.e solution GOR, Sm^3/Sm^3

s Skin factor

S_{cc} Critical condensate saturation

S_g Gas saturation

S_{gc} Critical gas saturation

S_{gn} Normalized, gas saturation

S_o Oil saturation

S_{wi} Irreducible water saturation

Δr_s Difference between gas entering Region 1 and the gas flowing at a given radial distance from the wellbore

t Time, days or hours

t_{eia} Time to the end of the infinite-acting period, days or hours

t_D Dimensionless time

t_{DA} Dimensionless time $(= t_D r_w^2/A)$

T_c Critical temperature, °C

T_{cri} Cricondentherm

T_g Empirical parameter for gas

T_o Empirical parameter for oil

T_{res} Reservoir temperature, °C or °R

T_{sc} Temperature at standard conditions, 15.56 °C or 60°F

V Molar volume

V_{ro} CCE oil relative volume, $V_o/(V_g + V_o)$

V_{ro} CVD oil relative volume, V_o/V_d

V_d Dewpoint volume, ft^3 *or* m^3

Z Compressibility factor

Z_g Gas Z-factor

Abbreviations

BHP Bottom Hole Pressure, $bars\ or\ psia$

BHFP Bottom Hole Flowing Pressure, $bars\ or\ psia$

CCE Constant Composition Expansion

CVD Constant Volume Depletion

CGR Condensate-Gas Ratio

EOS Equation of State

FBHP Flowing Bottom Hole Pressure, $bars\ or\ psia$

GOR Gas-Oil Ratio, Sm^3/Sm^3

HC Hydrocarbons

HPHT High Pressure High Temperatur

IFT Interfacial tension

LGR Liquid-Gas Ratio

LRS Liquid Rich Shale

OGR Oil-Gar Ratio, Sm^3/Sm^3

PTA Pressure Test Analysis

SRK Soave-Redlich-Kwong

STO Stock-tank-oil

Operators

Δ difference

Subscripts

c Critical

d dew point

D dimensionless

DA Dimensionless well drainage area

e external

eia end of infinite-acting period

g indicates to gas phase

i indicates initial

o indicates to oil phase

p producing

pD dimentionless producing

r radius

res reservoir

S saturation

sc standard condition

t total

w well

wf well flowing

Superscripts

$*$ Outer boundary

Symbols

ρ_g gas density

ρ_g oil density

ρ_w water density

μ_g gas viscosity, cP

μ_o oil viscosity, cP

$\emptyset$ porosity

γ Eulers constant

η diffusivity; similarity variable

∂ partial differential term

λ mobility